A comparison between experimental and calculated data shows that the ab initio force constants and intensities are fairly reliable. This justifies their use in cases where constants cannot be determined from experimental data alone. Secondly, it helps in choosing the correct set of force constants between sets which fit the observed data equally well.[12]

Acknowledgment. This work was supported by the Australian Research Grants Scheme. Dr. M. Rodler adknowledges the assistance of a Monash University Vice-Chancellor's Postdoctoral Fellowship.

Registry No. CCCO, 11127-17-6; $CCC^{18}O$, 11127-21-2; $CC^{13}CO$, 11127-20-1; $C^{13}CCO$, 11127-19-8; $^{13}CCCO$, 11127-18-7; $C^{13}C^{13}CO$, 11127-24-5; $^{13}CC^{13}CO$, 11127-23-4; fumaroyl dichloride, 627-63-4.

(11) Aliev, M. R. *Opt. Spectrosc.* **1971**, *31*, 301-304.
(12) McKean, D. C.; Duncan, J. L. *Spectrochim. Acta* **1971**, *27A*, 1879-1891.
(13) Herzberg, G. "Infrared and Raman Spectra"; D. Van Nostrand Co.: Princeton, NJ, 1945.

Direct Observation of Ion-Pair Dynamics

J. M. Masnovi and J. K. Kochi*

Contribution from the Chemistry Department, University of Houston, University Park, Houston, Texas 77004. *Received July 11, 1985*

Abstract: The intimate ion pair $[A^+,T^-]$ is spontaneously generated by the charge-transfer excitation of the electron donor–acceptor complex of anthracene donors (A) and tetranitromethane (TNO_2) with a 25-ps laser pulse. The kinetics of the subsequent ion-pair decay to the adduct (i.e., $[A^+,T^-] \rightarrow AT$) is followed spectroscopically over the separate picosecond, nanosecond, and microsecond time domains, each with a different laser-flash system. Three distinctive rate profiles are observed: (a) the picosecond decay following first-order kinetics (k_I), the nanosecond decay also following first-order but slower kinetics (k_{II}), and the microsecond decay following second-order kinetics (k_{III}). The experimental rate constants k_I, k_{II}, and k_{III} are associated with the relaxation of the intimate or tight ion pair $[A^+,T^-]$, the solvent-separated or loose ion pair $[A^+//T^-]$, and the free ions $[A^+ + T^-]$, respectively, as originally formulated by Winstein and co-workers for solvolysis mechanisms. These kinetics data together with the measurements of the fractional partitioning of ion pairs allow all the microscopic rate constants relevant to ion pair dynamics to be separately evaluated. The Winstein ion-pair formulation is substantiated by the observation and quantitative treatment of the "common-ion" and "special" salt effects. The role of solvent is underscored by the unique kinetics responses of reactive and persistent cations derived from various 9-substituted and 9,10-disubstituted anthracenes, respectively, with changes in the polarity of the medium from benzene and dichloromethane to acetonitrile. The overall importance of charge annihilation and separation in the microdynamics of transient ion pairs is underscored by a comparison with the bimolecular kinetics of radical–radical interaction measured under comparable conditions.

Ions and ion pairs are fundamental to our understanding of a wide variety of organic reaction mechanisms in solution.[1] Much of the knowledge about the behavior of stable ions derives largely from static conductometric measurements.[2] More recently, magnetic techniques such as NMR and ESR spectroscopy have been used to describe ion pairing and aggregation effects—principally still within a thermodynamic context.[3] Our understanding of the *dynamic* behavior of reactive ions and ion pairs stems largely from the pioneering investigations of solvolytic reactions by Winstein and co-workers.[4-7] Their elegant analysis of the solvolysis kinetics and observation of the "special" salt effects have led to the seminal concept of intimate and solvent-separated ion pairs as key reactive intermediates. Owing to the complexity of the kinetics, however, the general solutions of the rate expressions have not been sufficient to yield the microscopic rate constants for the various ion-pair dynamics.[8]

The development of laser-flash photolytic techniques especially on the picosecond time scale, now provides the experimental means to directly observe the complete spectrum of ion-pair dynamics.[9,10] Crucial to these studies is the spontaneous production of an ion pair in sufficient concentrations and in a discrete electronic state as well as geometric configuration to measure the relaxation kinetics in a homogeneous system.[11] We believe that the pro-

(1) (a) Hammett, L. P. "Physical Organic Chemistry", 2nd ed.; McGraw-Hill: New York, 1970. (b) Kosower, E. M. "An Introduction to Physical Organic Chemistry"; Wiley: New York, 1968. (c) Lowry, T. H.; Richardson, K. H. "Mechanism and Theory in Organic Chemistry", 2nd ed.; Harper & Row: New York, 1981. (d) Szwarc, M., Ed. "Ions and Ion Pairs in Organic Reactions"; Wiley-Interscience: New York, Vol. 1, 1972; Vol. 2, 1974.
(2) See, e.g.: (a) Schiavo, S.; Fuoss, R. M.; Marrosu, G.; Guida, G. *J. Solution Chem.* **1979**, *8*, 557 and references therein. (b) D'Aprano, A. *J. Solution Chem.* **1974**, *3*, 363. (c) Kaneko, H.; Wada, N. *J. Solution Chem.* **1978**, *7*, 19.
(3) For a review, see ref 1d, Chapters 5-8 in Vol. 1, p 177 ff.
(4) (a) Winstein, S.; Klinedinst, P. E., Jr.; Robinson, G. C. *J. Am. Chem. Soc.* **1961**, *83*, 885. (b) Winstein, S.; Klinedinst, P. E., Jr.; Clippinger, E. *J. Am. Chem. Soc.* **1961**, *83*, 4986. (c) Winstein, S.; Robinson, G. C. *J. Am. Chem. Soc.* **1958**, *80*, 169 and related papers. For reviews see: (d) Harris, J. M. *Prog. Phys. Org. Chem.* **1974**, *11*, 89. (e) Reference 1d, Vol. 2, Chapter 3, p 247 ff.
(5) Weiner, H.; Sneen, R. A. *J. Am. Chem. Soc.* **1965**, *87*, 287, 292. Sneen, R. A.; Larsen, J. W. *J. Am. Chem. Soc.* **1966**, *88*, 2593. Ogg, R. A., Jr.; Polanyi, M. *Trans. Faraday Soc.* **1935**, *31*, 604.
(6) (a) Goering, H. L.; Briody, E. G.; Levy, J. F. *J. Am. Chem. Soc.* **1963**, *85*, 3059. Goering, H. L.; Levy, J. F. *J. Am. Chem. Soc.* **1964**, *86*, 120. Young, W. G.; Winstein, S.; Goering, H. L. *J. Am. Chem. Soc.* **1951**, *73*, 1958. (b) Crampton, M. R.; Grunwald, E. *J. Am. Chem. Soc.* **1971**, *93*, 2987.
(7) See: Shiner, V. J., Jr.; in "Isotope Effects in Chemical Reactions"; Collins, C. J., Bowman, N. W., Eds.; Van Nostrand Reinhold: New York, 1970.
(8) Rather than individual rate constants, their ratios predominate.
(9) For example, see: Barbara, P. F.; Brus, L. F.; Rentzepis, P. M. *Chem. Phys. Lett.* **1980**, *64*, 447. Hochstrasser, R. P. *Pure Appl. Chem.* **1982**, *52*, 2683. Wang, Y.; Crawford, M. C.; Eisenthal, K. B. *J. Phys. Chem.* **1980**, *84*, 2696.
(10) (a) Simon, K. D.; Peters, K. S. *Acc. Chem. Res.* **1984**, *17*, 277. (b) See also: Goodman, J. L.; Peters, K. S. *J. Am. Chem. Soc.* **1985**, *107*, 1441.
(11) For example, flash photolysis of solvolytic systems have not been found to be useful since they are usually beset with a number of problems, including extraneous excited states and/or long-lived byproducts.[12]

0002-7863/85/1507-7880$01.50/0

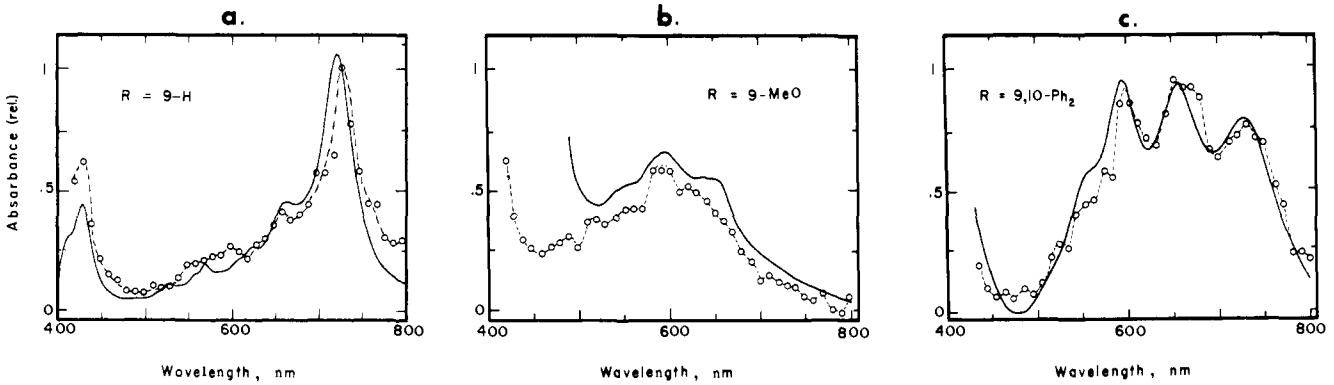

Figure 1. Comparison of the time-resolved transient (~30 μs) absorption spectrum of A^+ (-O-) from the CT excitation of the EDA complex with the steady-state absorption spectrum of A^+ (—) from the anodic oxidation of A for (a) anthracene, (b) 9-methoxyanthracene, and (c) 9,10-diphenylanthracene representing transient, semipersistent, and persistent cations, respectively. All measured in dichloromethane containing 0.1 M TBAP.

Table I. Absorption Spectra of Anthracene Cations[a]

9-R-,10-R′-anthracene	$\lambda_{max}(A^+)$, nm[b]	ϵ_{max}, M^{-1} cm^{-1} [c]	9-**R**-,10-R′-anthracene	$\lambda_{max}(A^+)$, nm[b]	ϵ_{max}, M^{-1} cm^{-1}, [c]
H, H	710	7700[d]	CH_3O, H	610	3800
CHO, H	735	*e*	Cl, CHO	750	2600
C_6H_5, H	720	(7700)[f]	CH_3, CHO	720	2500
Br, H	725	(7700)[f]	Cl, Cl	700	4000
CH_2=CH, H	690	(7700)[f]	Br, Br	710	3850
NO_2, H	760	*e*	C_6H_5, C_6H_5	660	9300
CN, H	770	*e*	CH_3, CH_3	650	4700

[a] In dichloromethane. [b] Determined from the spectra of cations generated by either CT excitation or anodic oxidation. [c] Evaluated as described in the Experimental Section. [d] From ref 22. [e] Too transient to measure. [f] Assumed value, see Experimental Section.

duction of ion pairs by charge-transfer (CT) excitation of electron donor–acceptor of EDA complexes fulfills these requirements.[13,14] Thus, we previously showed by time-resolved (picosecond) spectroscopy that the specific irradiation of the CT absorption bands of the EDA complexes of uncharged donors and acceptors results in electron transfer to produce the cation of the donor and the anion of the acceptor simultaneously, according to the expectations of Mulliken theory.[13] As applied to the 1:1 EDA complexes of a series of arene donors with tetranitromethane (TNM) as the common acceptor we found the CT irradiation to generate cleanly

$$A + TNM \overset{K}{\rightleftharpoons} [A,TNM] \qquad (1)$$

the arene cation (A^+) and the trinitromethide anion (T^-) within ~10 ps, i.e., the rise time of the 25-ps laser pulse.[15,16] Photo-

$$[A,TNM] \xrightarrow{h\nu_{CT}} [A^+,T^-,NO_2] \qquad (2)$$

chemical and product studies with various anthracene donors have established the subsequent (re)combination of the fragments (eq 2) to occur with high quantum yields via two sequential reactions,[17,18] viz.

$$A^+ + T^- \rightarrow AT \quad I \qquad (3)$$

$$AT + NO_2 \rightarrow AT\text{-}NO_2 \quad II \qquad (4)$$

Overall, the formation of the hydroanthryl intermediate I is tantamount to ion-pair collapse (eq 3). Similarly the production of the photoadduct II corresponds to radical recombination (eq 4). Thus, the time-resolved CT photochemistry of anthracene–TNM complexes provides us with an excellent opportunity to examine the dynamics of transient ion pairs and radical pairs in a single system concurrently.[19] In this study, we consider the sequential relaxation of the ion pair [A^+,T^-] over three distinctive time domains, viz., pico-, nano-, and microsecond, as it collapses to intermediate I in eq 3. The solvent and salt effects on the rates of such an ion-pair collapse are quantitatively compared with the dynamics of the subsequent disappearance of I by radical coupling (eq 4).

Results

I. Production of Ions by CT Excitation. The absorption spectra observed upon the CT excitation of anthracene–TNM complexes relate to the formation of the arene cations which typically exhibit strong absorptions in the visible region between 600 and 800 nm.[20] Figure 1 shows that the time-resolved microsecond spectra from

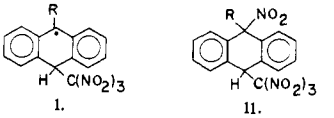

I. II.

(12) See: Cristol, S. J.; Stull, D. P.; McEntee, T. E. *J. Org. Chem.* **1978**, *43*, 1756 and references cited in footnote 2 of this paper.

(13) For charge-transfer theory, see: (a) Mulliken, R. S. *J. Am. Chem. Soc.* **1952**, *74*, 811. Mulliken, R. S.; Person, W. B. "Molecular Complexes: A Lecture and Reprint Volume"; Wiley: New York, 1969. (b) For a review, see: Foster, R. "Organic Charge Transfer Complexes"; Academic Press: New York, 1969.

(14) (a) Hilinski, E. F.; Masnovi, J. M.; Amatore, C.; Kochi, J. K.; Rentzepis, P. M. *J. Am. Chem. Soc.* **1983**, *105*, 6167. (b) Hilinski, E. F.; Masnovi, J. M.; Kochi, J. K.; Rentzepis, P. M. *J. Am. Chem. Soc.* **1984**, *106*, 8071.

(15) Masnovi, J. M.; Huffman, J. C.; Kochi, J. K.; Hilinski, E. F.; Rentzepis, P. M. *Chem. Phys. Lett.* **1984**, *106*, 20.

(16) In this system, electron transfer to the acceptor in essence occurs dissociatively, i.e., $TNM + e \rightarrow T^- + NO_2$. See: Bielski, B. H. J.; Allen, A. O. *J. Phys. Chem.* **1967**, *71*, 4544. See also: Rabani, J.; Mulac, W. A.; Matheson, M. S. *J. Phys. Chem.* **1965**, *69*, 53. Chaudhuri, S. A.; Asmus, K. D. *J. Phys. Chem.* **1972**, *76*, 26. See also: Glover, D. J. *Tetrahedron* **1963**, *19*, (Suppl. 1), 219.

(17) Masnovi, J. M.; Kochi, J. K.; Hilinski, E. F.; Rentzepis, P. M. *J. Am. Chem. Soc.*, submitted.

(18) Masnovi, J. M.; Kochi, J. K. *J. Org. Chem.*, in press. In these studies the arene donors consisted of mono- and disubstituted anthracenes with substituents (R) on the 9-, and 9,10- positions. The structures of the hydroanthryl intermediate **I** and the photoadduct **II** are

(19) (a) It is important to note that the CT excitation of the EDA complexes of anthracenes with TCNE[14] and TNM[15] are spectroscopically uncomplicated by the formation of other intermediate states or species, as observed on the picosecond time scale. (b) For a preliminary communication, see: Masnovi, J. M.; Levine, A.; Kochi, J. K. *J. Am. Chem. Soc.* **1985**, *106*, 4356. (c) Note that the absence of the nanosecond spectra in ref 19b precluded the observation of phase II. As a result, $F \simeq (F_{II} + F_{II}F_{III})/2$, $k_{obsd} = k_{III}$, $k_3 = k_{IV}$, and k_d/k_2 is now a composite of k_{-2}/k_2 and k_{-3}/k_3 in this paper.

(20) Masnovi, J. M.; Seddon, E. A.; Kochi, J. K. *Can. J. Chem.* **1984**, *62*, 2552.

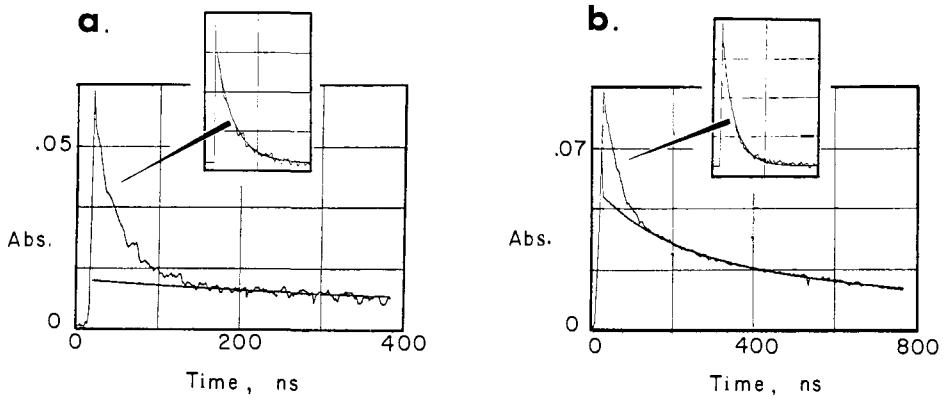

Figure 2. Typical nanosecond decay profiles of A^+ derived from the CT excitation at 532 nm of the EDA complex of 0.05 M A and 0.1 M TNM in CH_2Cl_2. Examples are for (a) anthracene and (b) 9-phenylanthracene. The lines are the computer-fitted least-squares treatment of the second-order base line (vide infra). The inset shows the first-order kinetics for the initial portion (<100 ns) of the decay profile.

three representative types of anthracenes are the same as the steady-state spectra of the corresponding cations generated by electrochemical oxidation. Moreover, these spectra coincide with the time-resolved picosecond spectra reported earlier,[15] as well as with the nanosecond spectra obtained at the intermediate time interval. In other words, the absorption spectra of these arene cations remain essentially unchanged as they evolve from their nascent ion-pair stage over a time span which covers more than 10 decades.[21] The absorption spectra of anthracene cations with 9-substituents such as bromo, phenyl, and vinyl are similar to the spectrum of the parent anthracene shown in Figure 1a, and the extinction coefficients at λ_{max} listed in Table I are also taken to be the same (vide infra). By comparison, the absorption spectrum of the cation derived from the electron-rich 9-methoxyanthracene shows a substantial blue-shift in Figure 1b. The 9,10-disubstituted anthracene cations, such as the diphenyl derivative shown in Figure 1c, are among the most persistent observed.

The trinitromethide anion T^- is formed simultaneously with the arene cation as a result of CT excitation of the arene–TNM complex in eq 2. The time-resolved absorption spectrum of T^- with λ_{max} 351 nm (ϵ 14 600 M^{-1} cm^{-1}) was previously demonstrated to be the same as that obtained during the electrochemical reduction of TNM.[17] Unfortunately the absorption band of T^- overlaps with the spectral region pertinent to the local excitation of the anthracene donors, which have intense aromatic absorptions between 350 and 400 nm.[20] Accordingly, we measured the temporal evolution of the ion pair $[A^+,T^-]$ by focusing on the spectral changes in the concentration of only A^+. The concentration of T^- was then taken implicitly to follow, i.e., $[A^+] = [T^-]$. Indeed the high yields of the hydroanthryl adduct I resulting from the bimolecular interaction of A^+ and T^- (see eq 3) provide excellent support for this premise.[23]

II. Time-Resolved Evolution of Ions. The use of three different pulsed-laser systems allowed us to monitor the subsequent relaxation of the ion pair $[A^+,T^-]$ for over three discrete time regimes—pico-, nano-, and microsecond which we designate as phases I, II, and III, respectively, of the ion-pair dynamics.[24] The time-resolved spectra in the region beween 500 and 800 nm reveal (a) the disappearance of the arene cation at ~750 nm and (b) the concomitant growth of the hydroanthryl intermediate I at ~550 nm (vide infra).

(21) Note that in this system consisting of large delocalized ions, we are unable to detect a measurable spectral shift of A^+ in the geminate ion pair compared to the free ion. Compare ref 10.

(22) Torikai, A.; Kato, R. *J. Polym. Sci., Polym. Chem.* **1978**, *16*, 1487.

(23) (a) High yields of **I** relate to the isolation in high yields of the ultimate photoadduct **II**.[18] Generally nitroform and other byproducts containing the trinitromethyl group were observed only in small amounts. (b) The concomitant formation of A^+ and T^- in a ~1:1 ratio was previously demonstrated[17] with A = hexamethylbenzene which is optically transparent in the region (λ = 350 ± 50 nm) where T^- absorbs.

(24) For a preliminary communication, see: Masnovi, J. M.; Levine, A.; Kochi, J. K. *Chem. Phys. Lett.*, in press.

Table II. Observed First-Order Rates of Disappearance of Arene Cations from the Intimate Ion Pair[a]

9-R-anthracene	k_I, s^{-1}	ref
H	1.5×10^9	*b*
NO_2	3.2×10^9	*b*
CHO	3.3×10^9	*b*
CN	3×10^9	*c*

[a] In dichloromethane at 20 °C. [b] As measured in ref 17. [c] See Experimental Section.

Table III. Fraction Survival and the Observed First-Order Rate Constant for the Second Decay Profile of Arene Cations[a]

9-R-anthracene	F_{II}[b]	k_{II}[c] s^{-1}
NO_2	<0.05	
H	0.37	2.7×10^7
Br	0.36	2.8×10^7
C_6H_5	0.64	1.7×10^7
CH_2=CH	0.53	1.1×10^7

[a] In dichloromethane at 20 °C, [A] = 0.05 M, [TNM] = 0.10 M. [b] From intensity measurements at 10 ns following CT excitation. [c] From the deconvolution of the biphasic decays observed between 10 and 200 ns.

A. Picosecond Kinetics in Phase I. The initial rate of disappearance of A^+ is highly dependent on the anthracene donors. Those anthracenes with electron-withdrawing substituents (R = NO_2, CHO, and CN) decay completely within 500 ps, whereas other anthracene cations (e.g., R = H and Ph) persist beyond 4 ns.[15] In the time interval of less than 500 ps, the disappearance of every A^+ follows first-order kinetics, as expected from the collapse of geminate species $[A^+,T^-]$ uncomplicated by diffusion. The observed first-order rate constants k_I are summarized in Table II.[17] The magnitudes of k_I depend on the 9-substituent, and they are the largest when R is the electron-withdrawing nitro or formyl group.

When the kinetics are monitored on the picosecond-flash system for longer than 4000 ps, a cation absorption can still remain. The intensity of the residual cation absorption is highly dependent on the anthracene, generally being the highest with the cations possessing electron-releasing substituents, as described below.

B. Nanosecond Kinetics in Phase II. The amount of arene cation remaining after 10 ns relative to that formed upon CT excitation was measured on the nanosecond-flash system after calibration of the laser output, as described in the Experimental Section. The results are reported as F_{II} in Table III. The value F_{II} = 0.37 for the anthracene cation (R = H) agrees well with the value of A_{4ns}/A_{50ps} = 0.4 obtained from the picosecond studies (vide supra) as the ratio of the residual absorbance remaining after 4 ns to the initial absorbance present at 50 ps following the laser flash.

The rate of disappearance of the residual cation absorptions after 10 ns is shown in Figure 2 for the arene cations derived from

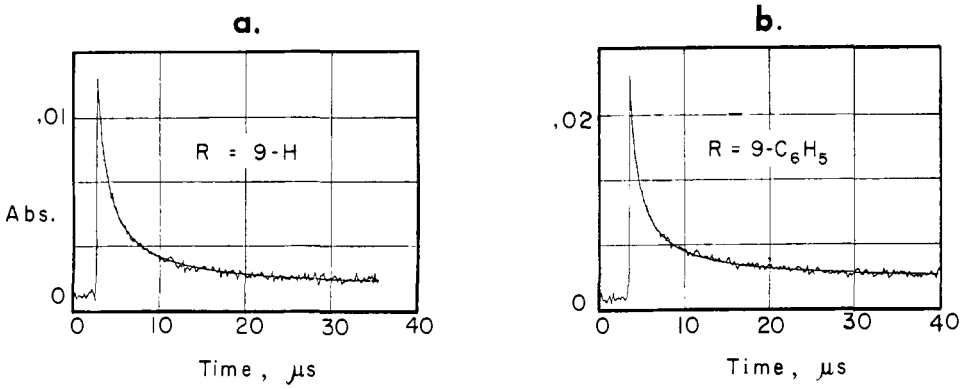

Figure 3. Typical microsecond decay profiles for A^+ (for the same pair in Figure 2). The smooth lines are the computer-fitted least-squares treatment of the rate data for second-order kinetics.

anthracene (R = H) and 9-phenylanthracene (R = C_6H_5) as two representative examples. The decay profile is biphasic for both cations. Thus, the kinetics analysis of the initial fast fall off of the absorbance reveals a first-order process with the rate constant $k_{II} = 2.7 \times 10^7$ s^{-1} for the anthracene cation (R = H). In general, the first-order rate constants (k_{II}) listed in Table III for this decay profile are several orders of magnitude slower than those (k_I) for the initial decay (compare with Table II).[19c]

The arene ions continue to disappear with first-order kinetics for about 100 ns after excitation. This is followed by a slower decay observed in the tail of Figure 2, which follows second-order kinetics, as described below.

C. Microsecond Kinetics in Phase III. At times longer than ~0.2 μs, the decay kinetics become clearly second-order. Thus, the time-resolved spectroscopy was carried on with the microsecond-flash system which generally covers the time interval from 1 to 100 μs after the CT excitation. A typical decay of the cation absorbance in this extended time interval is shown in Figure 3 for two representative examples. The smooth lines in the figures represent the computer-fitted least-squares treatment of the data for second-order kinetics. The second-order rate constant $k_{III} = 1.55 \times 10^{11}$ M^{-1} s^{-1} was obtained for the disappearance of the anthracene cation (R = H) based on the extinction coefficient of $\epsilon_{max} = 7700$ M^{-1} cm^{-1}.[22] Indeed this rate constant coincides with that (1.5×10^{11} M^{-1} s^{-1}) evaluated directly from the tail in Figure 2a in the time interval between 200 and 800 ns.

The excellent agreement of the two independent measurements of the second-order rate constant k_{III} substantiates the biphasic decay of the cation in the time interval of 10–400 ns (Figure 2). In fact, this long-lived, second-order component can be subtracted graphically from the experimental decay in Figure 2. The resulting difference decay presented in the inset obeys first-order kinetics, as shown by the coincidence with the smooth line based on the computer-fitted least-squares treatment. The first-order rate constant $k_{II} = 2.7 \times 10^7$ s^{-1} evaluated in this manner is identical with that obtained from the initial fast fall off (vide supra). Thus, the deconvolution of the biphasic decay in Figure 2 also provides reliable values of the first-order rate constant k_{II} and the second-order rate constant k_{III}.

The second-order rate constants k_{III} measured with the aid of the microsecond system for 9-substituted and 9,10-disubstituted anthracenes are listed in Table IV. The values of k_{III} are presented in the first column in absorbance units as obtained from the raw data. The second column presents the rate constants in more conventional units based on the best available values of ϵ_{max} for the various anthracene cations, as listed in Table I. Interestingly, the second-order rate constants k_{III} are not very sensitive to the nature of R, the values being essentially the same for R = Br, H, C_6H_5, and CH_2=CH. Only for those anthracene cations containing either the strongly stabilizing methoxy group or a pair of meso substituents is the value of k_{III} reduced.

The relative contribution of the first-order (k_{II}) and the second-order k_{III} processes in phases II and III, respectively, for the decay of arene cations is strongly dependent on the 9-substituent

Table IV. Observed Second-Order Rate Constants and the Fraction of the Third Decay Profile of Arene Cations[a]

9-R-,10-R′-anthracene	log k_{III}		F_{III}	F_{II}
	A^{-1} s^{-1}	M^{-1} s^{-1} [b]		
NO_2, H	c		<0.1	0.03
CN, H	c		<0.1	0.02
CHO, H	c		<0.1	0.05
H, H	7.62	11.2_0	0.19	0.37
C_6H_5, H	7.59	11.1_1	0.29	0.64
Br, H	7.64	11.2_2	0.19	0.36
CH_2=CH, H	7.57	11.1_5	0.37	0.53
CH_3O, H	6.3	9.6	1.0	1.0
Cl, Cl	5.6	8.9	1.0	1.0
Br, Br	5.9[d]	9.2	1.0	1.0
C_6H_5, C_6H_5	4.1	7.8	1.0	1.0
CH_3, CH_3	5.4	8.8	1.0	1.0

[a] In dichloromethane at 20 °C with [A] = 0.05 M, [TNM] = 0.10 M. [b] Calculated from results in column 2 and ϵ_{max} in Table I. [c] Signal too weak to treat reliably. [d] Decay appears to contain some first-order components.

R on anthracene. For example, the first-order process is dominant when R is hydrogen (Figure 2a), whereas the second-order process is dominant when R is phenyl or vinyl (Figure 2b). The ratio of the absorbance observed at ~0.2 μs to that observed at 10 ns represents the fraction of species undergoing second-order decay, and it is reported as F_{III} in Table IV. The values of F_{II} for a variety of anthracene cations are also included in the table for comparison.

Finally at times longer than 150 μs following the CT excitations, all the absorbing ionic species from 9-substituted anthracenes have disappeared, as evidenced by the return of the differential absorbance to the zero base line in the spectral region with λ_{max} ~700 nm. The transient absorption bands with λ_{max} ~550 nm arise from the hydroanthryl intermediate I (eq 3) as the absorptions of the ions disappear, and their dynamic behavior is included below.

III. Salt Effects on Ion-Pair Kinetics. The influence of salt on the ion-pair decay was examined with two types, in which the innocuous cation tetra-*n*-butylammonium (TBA) was paired with either the common anion T^- (i.e., TBAT) or the innocent anions,[25] perchlorate P^- (i.e., TBAP) and hexafluorophosphate H^- (i.e., TBAH). Two rate patterns emerge in a distinctive and dramatic way.

A. Innocent salts prolong the lifetime of arene cations in dichloromethane. Thus, Figure 4 illustrates the transformation of the 9,10-dibromoanthracene cation into a rather persistent species by the presence of 0.1 M tetra-*n*-butylammonium perchlorate (TBAP). Accordingly the quantitative analysis of the decay kinetics of various arene cations was carried out in the microsecond time domain. The results are presented in Figure 5 for the an-

(25) In our usage, "innocent" anions are "harmless in effect" (according to: "Webster's New Collegiate Dictionary", 7th ed.; G. C. Merriam: Springfield, MA) to the counterion A^+.

Table V. Effects of "Innocent Salt" on the Kinetics of Ion-Pair Decay[a]

9-R-,10-R′-anthracene	log k_{III} A^{-1} s^{-1}	log k_{III} M^{-1} s^{-1} [b]	F_{III}	9-R-,10-R′-anthracene	log k_{III} A^{-1} s^{-1}	log k_{III} M^{-1} s^{-1} [b]	F_{III}
NO_2, H	c		0.06	CH_3O, H	6.0	9.3	1.0
CN, H	d		0.05	Cl, Cl	4.1	7.4	1.0
CHO, H	c		0.09	CHO, Cl	c		1.0
H, H	5.4	9.0	0.70	CHO, CH_3	5.1	8.2	1.0
C_6H_5, H	5.5	9.1	0.81	Br, Br[d]	<5	<8	1.0
Br, H	5.5	9.1	0.66	C_6H_5, C_6H_5	4.1	7.8	1.0
CH_2=CH, H	5.5	9.1	0.75	CH_3, CH_3	5.3	8.7	1.0

[a] In dichloromethane containing 0.1 M [TNM], 0.05 M [A], and 0.1 M [TBAP] at 20 °C. [b] Calculated from the results in column 2 and ϵ_{max} in Table I. [c] Not determined. [d] Complex decay kinetics.

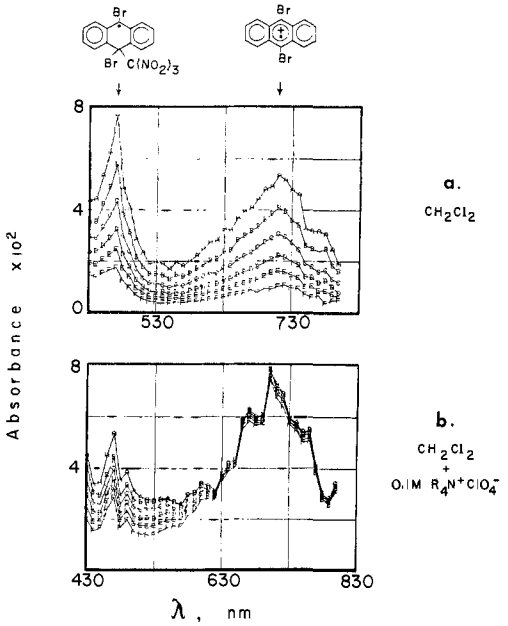

Figure 4. Salt effect on the time-resolved absorption spectrum derived from the CT excitation of 0.05 M, 9,10-dibromoanthracene and 0.10 M TNM in (a) dichloromethane alone and (b) dichloromethane containing 0.1 M TBAP taken at 5, 15, 30, 60, 90, and 140 μs following the laser pulse.

thracene cations with R = H and C_6H_5. Two features of the decay profiles are noteworthy. First, the disappearance of the arene cations follows second-order kinetics for the entire time interval from ~15 to 150 μs following the CT excitation, as shown by the coincidence of the decay profile with the computer-fitted line based on the second-order treatment of the data.[26] The magnitudes of the rate constants k_{III} listed in Table V are strongly reminiscent of those obtained in acetonitrile in the absence of salt (vide infra, Table VII). Second, the intensity of the initial absorption is affected little by the presence of 10 mM concentrations of TBAP. This is shown by the values of F_{III} in Table V which are not much greater than the values of F_{II} in Table IV.

The variation of the second-order rate constant k_{III} with the concentration of the added innocent salts TBAP and TBAH is illustrated in Figure 6. The sharp drop off of k_{III} at low concentrations of salt is noteworthy.

B. Common Ion in the form of either the tetra-*n*-butylammonium trinitromethide (TBAT) or the benzyltrimethylammonium trinitromethide (BM_3AT) salt eliminates the second-order decay of the cation absorption, while the first-order decays on the picosecond and nanosecond domains remain unaffected. The results of the addition of 10 mM TBAT on the decay of two representative anthracene cations are shown in Figure 7. The kinetics analysis of the rate profile shows a completely first-order process in the time interval of ~20–800 ns following CT excitation.[27] The first-order rate constants k_S at the optimum concentrations of TBAT are listed in Table VI for some anthracene cations. Note the similarity of the values of k_S and k_{II} in Table III.

Table VI. First-Order Rate Constants for Ion-Pair Decay in the Presence of the "Common Ion" T^- [a]

9-R-anthracene	salt,[b] mM	k_s(max),[c] s^{-1}
H	17	2.9×10^7
Br	25	2.7×10^7
C_6H_5	10	1.4×10^7
CH_2=CH	10	9.8×10^6

[a] In dichloromethane at 20 °C, [A] = 0.05 M, [TNM] = 0.10 M, [TBAT] ~ 0.010 M. [b] Concentration of TBAT at the maximum (see Figure 10.) [c] First-order rate constant at the maximum in Figure 10.

Table VII. Solvent Effect on the Kinetics of Ion-Pair Decay.[a] Removal of Phase II by Acetonitrile

9-R-,10-R′-anthracene	log k_{III} A^{-1} s^{-1}	log k_{III} M^{-1} s^{-1}	F_{III}
CHO, H	5.6	9.2	0.2
NO_2, H	c		0.1
H, H	5.6	9.2	0.73
C_6H_5, H	5.7	9.3	0.68
Br, H	5.5	9.1	0.69
CH_2=CH, H	5.3	8.1	0.63
CHO, Cl	5.4	8.5	1.0
CHO, CH_3	5.1	8.3	1.0
Br, Br	5.1[d]	8.3	1.0
C_6H_5, C_6H_5	4.1	7.8	1.0
CH_3, CH_3	5.4	8.8	1.0

[a] In acetonitrile containing 0.1 M [TNM] and 0.05 M [A] at 20 °C. [b] Calculated from the results in column 2 and ϵ_{max} in Table I. [c] Complex decay kinetics. [d] Decay appears to contain an appreciable first-order component.

IV. Solvent Effects on Ion-Pair Kinetics. Solvent polarity plays an important but selective role in the time-resolved spectral changes. For example, with 9-formylanthracene, the lifetime of the cation is too short in the nonpolar dichloromethane to observe on the microsecond time scale (vide supra). By contrast, when the same cation is generated in the more polar acetonitrile, absorptions can be readily observed under equivalent conditions. This solvent effect is dramatically illustrated in Figure 8 by the series of time-resolved spectra commencing at 10 μs after CT excitation (and subsequently at the periodic intervals given in the legend). On the extended time scale, the arene cation has clearly decayed completely in dichloromethane, and only the slower subsequent disappearance of the hydroanthryl adduct I is apparent. However, in acetonitrile, the arene cation is initially a prominent species, and its decay parallels that of I.

The decay of the various anthracene cations in the more polar acetonitrile follows second-order kinetics for the entire time interval between 15 ns and 160 μs following the CT-excitation pulse.[26] In this regard, the kinetics behavior is the same as that observed above in dichloromethane with added innocent salt. The second-order rate constants k_{III} measured in acetonitrile are listed in Table VII for various anthracene derivatives.

(26) Although the figure covers a limited time span, the rate profile was also independently examined at <1 μs and >160 μs for second-order behavior.

(27) As indicated in the figure, the decay has been independently observed to have reached the base line beyond 800 ns.

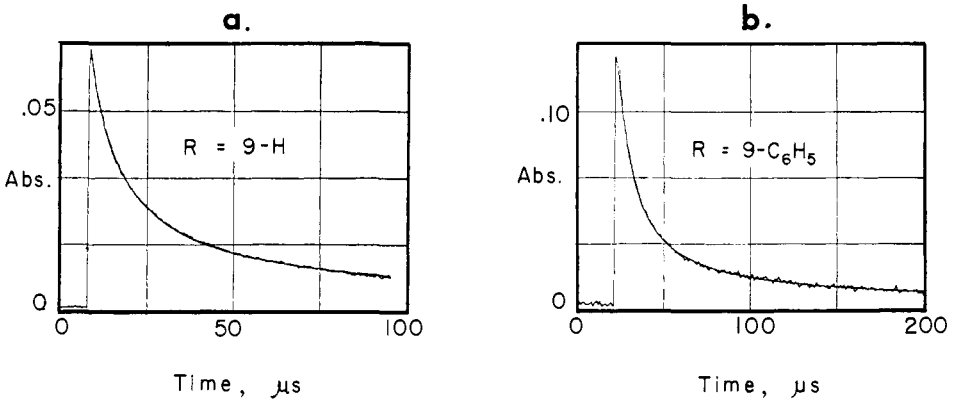

Figure 5. Effect of "innocent" salts on the decay profile of A^+ in dichloromethane during the CT excitation of 0.10 M TNM and (a) 0.05 M anthracene and (b) 0.05 M 9-phenylanthracene containing 0.1 M TBAP. The smooth line represents the computer-fitted least-squares treatment of the rate data for second-order kinetics.

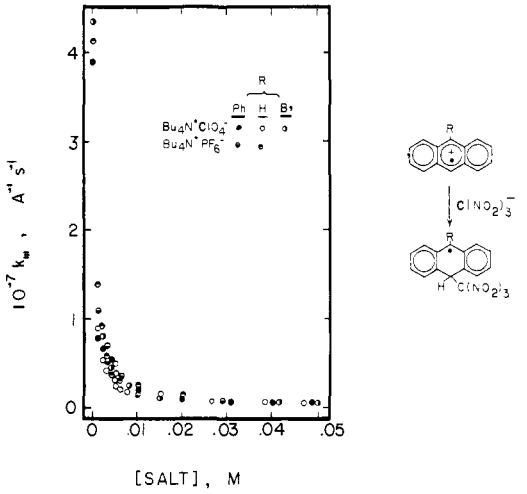

Figure 6. Effect of the concentration of "innocent salts" TBAP and TBAH on the experimental rate constant k_{III} of various anthracene cations in dichloromethane.

Unlike the kinetics observed in dichloromethane, the addition of the innocent salt TBAP to acetonitrile had no significant influence on the decay of A^+ even up to 500 mM. Similarly, the addition of the common-ion salt TBAT at normal levels (i.e., 10 mM) to acetonitrile had little effect on the decay profile. However, at high concentrations of TBAT (500 mM), the kinetics behavior approached first-order in a somewhat complex manner which we did not examine further.

Benzene at the other extreme of solvent polarity clearly delineates the slow decay of the persistent arene cations derived from the 9,10 disubstituted anthracenes. Thus, these cations remain essentially unchanged in dichloromethane on the microsecond time scale, as indicated by the F_{III} values of unity in Table IV. Their slow subsequent decay only follows second-order kinetics (k_{III}) typical of phase III—the first-order components k_I and k_{II} in phase I and II, respectively, being singularly absent or too slow to measure. However, in benzene, the same persistent cations disappear rather rapidly by largely first-order kinetics. The first-order rate constant k_{II} in Table VIII for the persistent cations in benzene is approximately 2 orders of magnitude slower than the values of k_{II} listed in Tables III and VI for the more reactive arene cations. It is important to note that the persistent arene cations respond in benzene to the presence of "common ion" and "innocent" salts in much the same way as their more reactive counterparts. Thus, small amounts (1–4 mM) of TBAP dramatically alter the decay profiles to second-order behavior (k_{III}). Substitution with TBAT restores clean first-order kinetics with the same rate constant k_{II} as that obtained in the absence of the common ion (Table VIII).

Table VIII. Solvent Effect. Restoration of Phase II for Persistent Arene Cations by Benzene[a]

9-R-,10-R-anthracene	no salt log k_{II}[b]	TBAP log k_{III}[c]	TBAT log k_{II}[d]
CH_3, CH_3	5.3	5.0 (8.4)[e]	5.0
C_6H_5, C_6H_5	5.6	5.0 (8.7)[f]	5.4

[a] Major kinetics component given as k_{II} (first-order) or k_{III} (second-order) from benzene solutions containing 0.1 M [TNM] and 0.05 M [A] at 20 °C. [b] In s^{-1}. [c] 1–4 mM TBAP in benzene, in $A^{-1} s^{-1}$. [d] 1–4 mM TBAT in benzene, in s^{-1}. [e] Value in parenthesis in $M^{-1} s^{-1}$ assuming ϵ_{660} = 4700 $M^{-1} cm^{-1}$. [f] Value in parentheses in $M^{-1} s^{-1}$ assuming ϵ_{660} = 9300 $M^{-1} s^{-1}$.

V. Radical-Pair Kinetics (Phase IV). The kinetics of ion-pair decay cascading through Phases I, II, and III as described above, all relate to the formation of the hydroanthryl radical adduct I (see eq 3). The identity of I as an intermediate can be demonstrated by its absorption spectrum observed after the transient

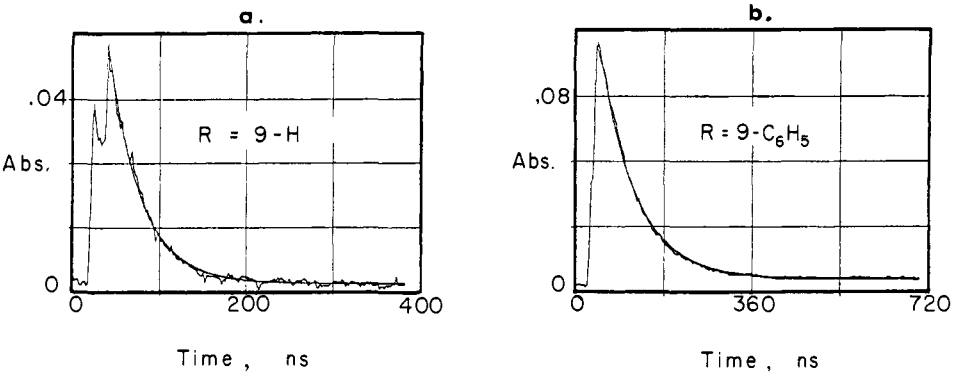

Figure 7. "Common ion" effect on the decay of A^+ in dichloromethane during the CT excitation of 0.10 M TNM and 0.05 M (a) anthracene and (b) 9-phenylanthracene containing 0.1 M TBAT. The smooth line represents the computer-fitted least-squares treatment of the rate data for first-order kinetics.

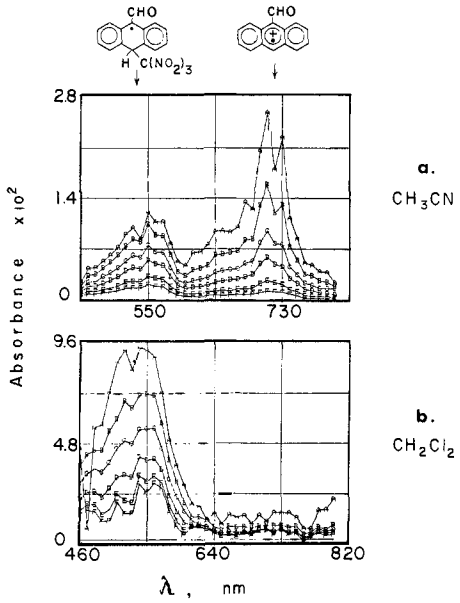

Figure 8. Solvent effect on the time-resolved absorption spectrum derived from the CT excitation of 0.10 M TNM and 9-anthraldehyde (a) saturated (~0.01 M) in acetonitrile and (b) 0.05 M in dichloromethane taken at 3, 9, 15, 25, 40, and 60 μs following the laser pulse.

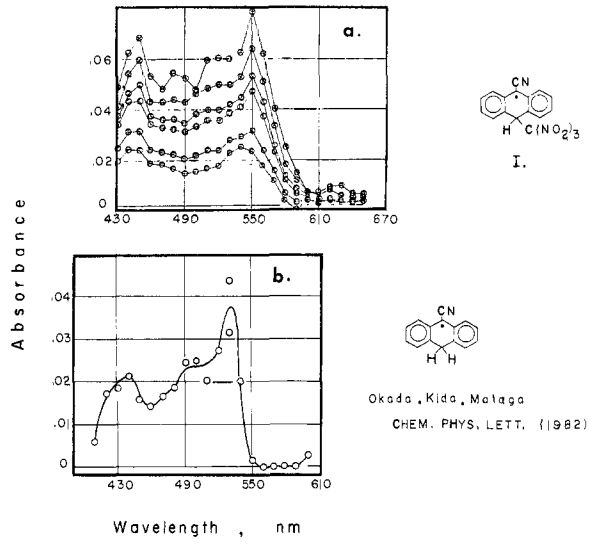

Figure 9. (a) Time-resolved absorption spectrum of the hydroanthryl intermediate **I** derived from the CT excitation of 0.05 M 9-cyanoanthracene and 0.10 M TNM in dichloromethane taken at 2, 10, 16, 27, 42, and 62 ns following the laser pulse. (b) Transient absorption spectrum of the 9-cyanohydroanthryl radical from the pulse radiolysis of 9-cyanoanthracene in ethanol containing 1% vol H_2SO_4 reproduced from ref 28 on the same wavelength scale.

absorptions due to the full decay of the arene cations. Figure 9a includes the time-resolved absorption spectrum of the hydroanthryl adduct **I** derived from 9-cyanoanthracene. The subsequent disappearance of the hydroanthryl intermediate is shown by the absorbance changes in the sequential spectra taken at 10–15-μs intervals. These hydroanthryl intermediates are generally characterized by absorption bands with $\lambda_{max} \sim 550$ nm. The structural assignment is confirmed by comparison of the spectrum of the cyano analogue with that of the related 9-cyanohydroanthryl radical previously generated by Mataga et al.[28] and reproduced in Figure 9b for comparison. The observation of the hydroanthryl intermediate following the decay of the arene cation absorptions indicates that they are formed irreversibly. Furthermore, the isolation of the photoadduct II (eq 4) in high yields from 9-substituted anthracenes demonstrates that the hydroanthryl radical **I** is the key intermediate.[29]

(28) Okada, T.; Kida, K.; Mataga, N. *Chem. Phys. Lett.* **1982**, *88*, 157.

Table IX. Observed Rate Constants for the Decay of the Hydroanthryl Adduct **I**[a]

9-R-,10-R-anthracene	λ_{max}, ϵ_{max}, nm M^{-1} cm^{-1}	log k_{IV}[b] CH_2Cl_2	CH_2Cl_2-(TBAP)	CH_3CN
NO_2, H	550 (1500)[c]	5.5 (8.4)	5.9 (8.8)	5.6 (8.5)
CN, H	545 (2400)[c]	5.8 (8.9)	5.8 (8.9)	5.8 (8.9)
CHO, H	545 *d*	5.7	6.1	5.7
CHO, CH_3	560 *d*	6.1	*e*	*e*

[a] Under the conditions in Table IV. [b] In A^{-1} s^{-1} (values in parentheses in M^{-1} s^{-1}). [c] Using ϵ_{max} for A^+ in Table I. [d] Not determined. [e] Overlaps absorptions due to A^+.

Scheme I

$$RX \underset{k_1}{\overset{k_{-1}}{\rightleftharpoons}} [R^+,X^-] \underset{k_2}{\overset{k_{-2}}{\rightleftharpoons}} [R^+ /\!/ X^-] \underset{k_3}{\overset{k_{-3}}{\rightleftharpoons}} R^+ + X^-$$

$[R^+ /\!/ X^-] \downarrow S$; $R^+ + X^- \downarrow S$

Scheme II

$$\underset{\text{adduct}}{I} \underset{k_1}{\overset{k_{-1}}{\rightleftharpoons}} \underset{\text{intimate i.p.}}{[A^+,T^-]} \underset{k_2}{\overset{k_{-2}}{\rightleftharpoons}} \underset{\text{"loose" i.p.}}{[A^+ /\!/ T^-]} \underset{k_3}{\overset{k_{-3}}{\rightleftharpoons}} \underset{\text{"free" ions}}{A^+ + T^-}$$

The radical combination of the hydroanthryl intermediate with nitrogen dioxide (eq 4) represents the final stage for the formation of photoadduct **II** following the CT excitation of the EDA complex. The kinetics analysis of the series of time-resolved spectra such as those illustrated in Figures 4, 8, and 9a indicates that the hydroanthryl radical disappears with second-order kinetics. The second-order rate constants k_{IV} are listed in Table IX for some representative derivatives in both dichloromethane and acetonitrile solvents and in the presence of added salt (TBAP).

Discussion

The interaction of the arene cation A^+ and the trinitromethide anion T^- to afford the neutral hydroanthryl adduct I as given in eq 3 formally represents the microscopic reverse of the heterolytic dissociations commonly encountered in organic reactions.[1] Indeed the dynamics of both processes are dominated by the energetics of charge annihilation (or separation) in ion pairs as an important part of a common driving force.

I. Dynamics of Transient Ions and Ion Pairs. Since the ion-pair dynamics involved in heterolytic dissociation have been thoroughly and rigorously examined in solvolysis reactions, we draw upon the general mechanism summarized in Scheme I.[4-7,30]

In this formulation, the reactant RX initially suffers heterolysis to the intimate ion pair $[R^+,X^-]$. This ion pair can collapse and regenerate RX, or relax to a solvent-separated or "loose" ion pair $[R^+//X^-]$. The latter in turn can re-form the intimate ion pair, dissociate to "free" ions $[R^+ + X^-]$, or be trapped by the solvent (i.e., solvolysis). Likewise, the free ions can reassociate to the loose ion pair or be trapped by solvent nucleophiles.

The presence of three ionic intermediates in Scheme I is akin to the three distinct ion-pair dynamics observed in phases I, II, and III of this study. We thus formulate our results within the same mechanistic framework as shown in Scheme II.

For Scheme II, our studies commence with the spontaneous appearance of $[A^+,T^-]$ which is the intimate ion pair. Thus, the vertical CT excitation of the EDA complex in eq 2 ensures that the ions A^+ and T^- are born as a discrete ion pair,[31] the mean separation of which is dictated by the geometry extant in the precursor complex.[32] Accordingly, the picosecond spectra record

(29) The formation of photoadduct **II** must proceed via the hydroanthryl radical **I**.[18]

(30) Note that the rate constants in Scheme I are designated according to the notation used in Scheme II.

(31) Within the time resolution of ≤3 ps required for the dissociative electron attachment of TNM to produce T^- and NO_2, as described in ref 15 and 17.

Table X. Rates of Elementary Processes for Arene Cations with Trinitromethide[a]

9-R,10-R′-anthracene	k_1, s^{-1} [b]	k_{-2}/k_1 [c]	k_{-2}, s^{-1} [c]	k_2, s^{-1} [d]	k_{-3}, s^{-1} [e]	k_3, M^{-1} s^{-1} [f]	k_3/k_{-3}, M^{-1}
H	1.5×10^9	0.58	8.7×10^8	4.3×10^7	6.4×10^6	2.0×10^{11}	3.1×10^4
Br		0.57		4.6×10^7	6.9×10^6	2.1×10^{11}	3.0×10^4
C_6H_5		1.8		3.9×10^7	5.7×10^6	2.1×10^{11}	3.7×10^4
CH_2=CH		1.1		2.1×10^7	5.8×10^6	2.3×10^{11}	4.7×10^4
NO_2	3.2×10^9	0.03	9.9×10^7				
CHO	3.3×10^9	0.05	1.7×10^8				
CN	3×10^9	0.02	6×10^7				

[a] At 20 °C in CH_2Cl_2, [An] = 0.05 M, [TNM] = 0.1 M. [b] From ref 17. [c] Determined from F_{II}, Table II. [d] Calculated from eq 5. [e] Determined from F_{III}, Table IV. [f] Calculated from eq 7, assuming ϵ_{max} = 7700 M^{-1} cm^{-1} (ref 22)8 l = 0.5 cm.[34]

the intimate ion pairs $[A^+,T^-]$ initially trapped within the solvent cage, since the observation on this time scale obviates from consideration of any competition from diffusional processes.

II. Microscopic Rate Constants for the Elementary Processes in Ion-Pair Dynamics. The intimate ion pair $[A^+,T^-]$ in Scheme II collapses on the picosecond time scale with the first-order rate constant k_1 to the hydroanthryl intermediate I in competition with the first-order relaxation (k_{-2}) to the "loose" ion pair.

The residual ion absorption remaining after 4 ns is ascribed to the loose ion pairs. The value of k_{-2} can then be determined from the fraction of intimate ion pairs which relax to the loose ion pairs, i.e., $F_2 = k_{-2}/(k_1 + k_{-2})$, which is given by the measured value F_{II} in Tables III and IV. The loose ion pairs also decay with first-order kinetics, albeit on the slower nanosecond time scale to form the hydroanthryl adduct I. The process logically proceeds via the re-formation of the intimate ion pair. Accordingly, the microscopic rate constant for this process (k_2) can be obtained from the experimental rate constant k_{II} relating to the loose ion pair and the Bodenstein steady-state approximation[1a] as eq 5.

$$k_2 = k_{II}/(1 - F_{II}) \tag{5}$$

At the same time, the loose ion pair dissociates to the free ions with rate constant k_{-3}. The value of k_{-3} is determined by the fraction of loose ion pairs which ultimately affords free ions and decays by second-order kinetics, i.e., $F_3 = k_{-3}/(k_2 + k_{-3})$. Since the recycling through the intimate ion pair is relatively rapid (k_2, $k_{-2} > k_{-3}$), the correction can be explicitly taken into account as eq 6.[33] This correction is small (i.e., $1.0 < F_{III}/F_3 < 1.7$) for

$$F_{III} = F_3 \sum_{n=0}^{\infty} [F_2(1 - F_3)]^n = F_3[1 - F_2(1 - F_3)]^{-1} \tag{6}$$

the 9-substituted anthracenes of interest in Table III.

Finally, the combination of free ions A^+ and T^- occurs with second-order kinetics to re-form the ion pairs (and ultimately to yield the hydroanthryl adduct I). The rate constant k_3 for this process can be obtained from the observed second-order rate constant k_{III} and the disposition of ions from the two ion-pair intermediates by invoking steady-state kinetics,[1a,34] i.e.,

$$k_3 = k_{III}[1 + (1 - F_2)^{-1}\{(1 - F_3)^{-1} - 1\}] \tag{7}$$

The foregoing relationships were used to convert the experimental rate constants k_1, k_{II}, and k_{III} listed in Tables II, III, and IV, respectively, together with the experimental fractions F_{II} and F_{III}, to the individual rate constants pertaining to each of the elementary processes in Scheme II. The resulting values of the microscopic rate constants are collected in Table X for various anthracene cations.

III. Nature of the Elementary Processes. The availability of these rate constants provides an opportunity to shed light on the nature of the elementary processes in ion-pair dynamics. Moreover, the anthracene cation is an ideal representative for these studies, since it is large and its cationic reactivity is readily tuned by meso substituents. Thus, anthracene cations have a high charge density centered at the 9,10- or meso position.[35] They are very sensitive to the effects of meso substituents,[36] and the presence of an electron-donating group at these positions strongly stabilizes the cation. Likewise, electron-attracting substituents destabilize the cation. Changes in the reactivity of the arene cation are reflected accordingly. For example, in Scheme II, the rates of these processes leading to charge annihilation (k_1) and tight ion pairing (k_2) decrease as the donor strength of the meso substituent increases. Contrariwise, the process involving charge separation (k_{-2}) increases. The rates are also sensitive to steric effects. The meso-disubstituted anthracene cations decay more slowly and have higher fractions which escape ion-pair collapse (i.e., larger values of F_{II} and F_{III}) than do their monosubstituted counterparts (cf. 9-Br with 9,10-Br,Br).

The behavior of the "free" ions in Scheme II is reflected in the bimolecular rate constant k_3. The magnitudes of k_3 are very large and are similar for all the monosubstituted anthracenes—reflecting the diffusion-limited character of the ionic combination. Indeed, the values of $k_3 \geq 2 \times 10^{11}$ M^{-1} s^{-1} in Table X are about an order of magnitude greater than that expected for the diffusional encounter of uncharged species. [The latter can be evaluated as $\sim 1.5 \times 10^{10}$ M^{-1} s^{-1} from the rate of π-dimerization of the anthracene cation with its neutral counterpart, and it is consistent with the rate based on the modified Debye equation, $k_d = 8RT/(3000\eta)$ where η is the bulk viscosity of the solvent.[37]] The higher rate of ion-pair collapse can be rationalized on the basis of an added component arising from the electrostatic attraction of oppositely charged ions. The inclusion of such a Coulombic effect with Fick's law of diffusion leads to an estimate of the incremental effect as

$$k_d^{+,1}/k_d^{0,0} = r_0/R \tag{8}$$

where R is the reaction radius of the uncharged species and $r_0 = e^2/(DkT)$.[38] An enhancement factor of $r_0/R \simeq 12$ is predicted from eq 8 if R is taken as 5 Å[38] and the dielectric constant D = 9.08.[39]

(32) For the mean separations in weak EDA complexes of the type described here, see: Fukuzumi, S.; Kochi, J. K. *J. Phys. Chem.* **1980**, *84*, 608 and related papers. For some ambiguity in the An–TNM complex, see footnote 21 in ref 18.

(33) See Experimental Section for the derivation of eq 6.

(34) (a) Note that if k_{III} is given in absorbance units, it must be multiplied by the extinction coefficient ϵ_{max} and the optical path length l for its conversion to concentration units c (i.e., using Beer's law, $A = \epsilon cl$.) (b) In this formulation, it is assumed that the free ions yield I via the intimate ion pair to accord with chemical reversibility in Scheme I. Although not favored, there is an alternative possibility in the scheme in which the intimate ion pair is bypassed,

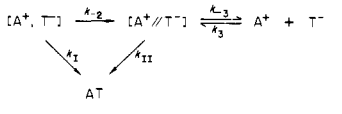

or another intimate ion pair different from the geminate ion produced in the CT excitation is involved. (For example, one difference might arise from the presence of NO_2 in the geminate ion cage, but NO_2 should not be present after internal or external return.)

(35) Coulson, C. A.; Streitwieser, A., Jr.; Brauman, J. I. "Dictionary of PiElectron Calculations"; Pergamon Press: Oxford, England, 1965.

(36) (a) Klasinc, L.; Kovač, B.; Güsten, H. *Pure Appl. Chem.* **1983**, *55*, 289. (b) See also ref 20.

(37) (a) Gordon, A. J.; Ford, R. A. "The Chemist's Companion"; Wiley: New York, 1972; pp 136–67. Compare also: Ritchie, C. D.; Vanverth, J. E.; Virtanen, P. O. I. *J. Am. Chem. Soc.* **1982**, *104*, 3491 and related papers. (b) Debye, P. *Trans. Electrochem. Soc.* **1942**, *82*, 265.

(38) Weston, R. E., Jr.; Schwarz, H. A. "Chemical Kinetics"; Prentice Hall: Englewood Cliffs, NJ, 1972; p 151 ff.

(39) Weast, R. C., Ed. "Handbook of Chemistry and Physics", 55th ed.; CRC Press: Cleveland, OH, 1974; p 56. The diffusion constants for ions expected to be the same (or slightly smaller) than those for neutral molecules: Shushin, A. I. *Chem. Phys. Lett.* **1985**, *118*, 197.

Scheme III

loose ion-pair exchange

$$[A^+//T^-] + [TBA^+//X^-] \underset{k_T}{\overset{k_X}{\rightleftharpoons}} [A^+//X^-] + [TBA^+//T^-]$$

intimate ion-pair exchange

$$[A^+, T^-] + [TBA^+//X^-] \underset{k_T'}{\overset{k_X'}{\rightleftharpoons}} [A^+, X^-] + [TBA^+//T^-]$$

free ion exchange

$$A^+ + X^- \underset{k_3'}{\overset{k_{-3}}{\rightleftharpoons}} [A^+//X^-]$$

The association of the "free" ions to form the loose ion pair, as given by the formation constant $K_3 = k_3/k_{-3}$, is singularly independent of the 9-substituent on anthracene. This unique behavior is consistent with the concept of loose ion pairs in which the cation experiences only a nonspecific Coulombic interaction with the counterion. At the low concentrations of ions involved, the Fuoss relationship provides an estimate of the interaction radius of such a loose ion pair.[40]

The equilibrium between the loose ion pair and the intimate ion pair is given by $K_2 = k_2/k_{-2}$, the value of which is presently available only for R = H. We judge from the magnitude of the association constant $K_2 = 0.047$ that the loose ion pair from anthracene is favored over the tight ion pair by $\Delta G \simeq 2$ kcal mol^{-1}. This difference is sufficient to neglect operationally the small concentrations of intimate ion pairs. Unlike K_3, the magnitude of K_2 is expected to depend on the nature of the ions. In particular, given the large changes observed in the F_{II} values and the low sensitivity of k_1 (and k_2) to changes in the donor, we expect the substantial differences in K_2 to arise principally from changes in k_{-2}.

IV. Direct Observation of the "Common Ion" and "Special Salt" Effects. Salt effects have provided an important role for the ion-pair mechanism in Scheme I for solvolysis—first as the "common ion" effect and second as the "special salt" effect.[41] Likewise, the dramatic and distinctive salt effects reported in Tables V and VI are readily interpreted in light of the ion-pair dynamics in Scheme II. In fact, we believe that the unique response of the kinetics to both types of salts provides compelling support for the essential correctness of the ion-pair mechanism in Scheme II (and in Scheme I).[30] Central to the formulation of salt effects is the exchange of the counterions through the intermediacy of the loose ion pair, the intimate ion pair, and the free ions, as outlined in Scheme III.[42,43] Let us consider separately the addition of salt which introduces either the "common ion" T^- or the "innocent ion" X^- (where X^- = perchlorate or hexafluorophosphate).

A. Common Ion Effect. The presence of the common ion T^- in the form of TBAT has a dramatic effect on the complexion of the ion-pair decay. Most importantly, the complete elimination

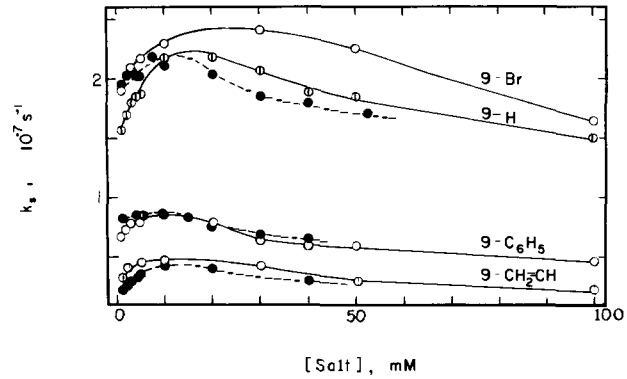

Figure 10. Concentration dependence on the "common ion" effect as measured by the first-order rate constant k_S in dichloromethane for 9-bromo-, 9-phenyl-, 9-vinylanthracene, and anthracene with added TBAT (○) and BM_3AT (●).

of the second-order decay k_{III} typical of phase III (see Figure 7) indicates that any free A^+ becomes highly ion paired, i.e.

$$A^+ + [TBA^+//T^-] \rightleftharpoons [A^+//T^-] + TBA^+ \qquad (9)$$

upon the addition of as little as 10 mM TBAT. Such a conclusion is in complete accord with the resultant, clean first-order kinetics observed for the cation decay in the time interval of 20–800 ns following the CT excitation. [The return of the differential absorption to the zero base line (see Figure 7) after 800 ns underscores the absence of the slower second-order component under these conditions.] The first-order rate constant k_S obtained with added TBAT is almost independent of the concentration of added TBAT, as shown in Figure 10. Most compellingly, the magnitude of k_S at optimum concentrations of TBAT (i.e., the maximum in Figure 10) is identical with the measured rate constant (k_{II}) for the loose ion pair in the absence of salt. (See eq 9 and compare the results in Table VI with those in Table III.) The rising portion of the curve in Figure 10 relates to increasing ion-pair saturation as described in eq 9.[44] On this basis, an estimate of the association constant $K_3 \sim 5 \times 10^3$ M^{-1} is obtained at the maximum. This value agrees reasonably well with the value of $K_3 = 3 \times 10^4$ M^{-1} obtained from the kinetic analysis as k_3/k_{-3}, especially if one considers the nature of the experimental difficulties. The slow fall off of k_S in Figure 10 at higher salt concentrations is ascribed to a normal salt effect.

B. Special Salt Effect. The kinetics behavior in the presence of an added innocent salt TBAX stands in strong contrast to the common ion effect described above. Thus, the residual absorptions now decay completely by slow second-order kinetics for the *entire* interval from ~15 ns to 160 μs (Figure 5). The marked absence of the first-order component k_{II} typical of phase II upon the addition of TBAX arises from the competitive scavenging of the loose ion pair by the innocent salt, i.e.

$$[A^+//T^-] + [TBA^+//X^-] \underset{k_T}{\overset{k_X}{\rightleftharpoons}} [A^+//X^-] + [TBA^+//T^-] \qquad (10)$$

Such an exchange effectively converts the chemically active ion pair $[A^+//T^-]$ into an unreactive ion pair $[A^+//X^-]$, which is kinetically akin to the dissociation into the free ion A^+.[46] The more or less complete interception of the loose ion pair $[A^+//T^-]$ by 10 mM TBAX (Figure 6) within ~15 ns suggests that the

(40) The interaction radius a of the ions can be estimated by the Fuoss equation $[K_3 = 4\pi Na^3/3000 \exp(2r_0/a)]$ at the low concentrations of the free ions involved (~10^{-5} M). With $K_3 \simeq 3 \times 10^4$ M^{-1}, $a = 1.9 \times 10^{-6}$ cm, indicating a mean separation of ~ 100 Å for the loose ion pair. [See: Justice, M. C.; Justice, J.-C. *J. Solution Chem.* **1976**, *5*, 543.] A simplification of the Bjerrum model, which apparently affords thermodynamic results in closer agreement with experiments [Denison, J. T.; Ramsey, J. B. *J. Am. Chem. Soc.* **1955**, *77*, 2615], affords $-\ln K = e^2/aDkT$ and $a = 5.13$ Å. We thank a referee for reference to this work. Whereas the latter value for a seems too low, the former is certainly too high, as judged by the different slopes in Figure 11 (which likely is due to specific effects of the different ions). We include these values as an indication of the present level of theory in describing ionic interactions.

(41) For a succinct summary, see ref 1c, p 320 ff.

(42) Exchange via the intimate or tight ion pair to produce another tight ion pair or a loose ion pair is also possible.[10] For simplicity, we do not distinguish between these pathways. It is noteworthy that in solvolysis mechanisms, exchange involving tight ion pair is believed to contribute negligibly to the trapping of organic cations.[43]

(43) See ref 4–7. The results in Table V indicate that 0.1 M TBAP in dichloromethane traps the intimate ion pairs with ~50% efficiency. The structure of intimate ion pairs involving a large, delocalized ion of the type examined here may however differ somewhat from those obtained in solvolysis studies.

(44) A similar behavior is observed with the unsymmetric BM_3AT, although the maximum in k_s in Figure 10 occurs at lower concentrations than that observed with TBAT. Nonetheless, the magnitudes of the rate constant k_s at the maxima are the same for both trinitromethide salts. The observation of k_s(max) at lower concentrations of BM_3AT may indicate weaker association of T^- with BM_3A^+ than with TBA^+ although the opposite is known for some anions.[45]

(45) Smid, J. ref 1d, Vol. 1, Chapter 3, pp 86–151.

(46) The unreactivity of $[A^+//X^-]$ is demonstrated by the electrochemical reversibility of the anodic oxidation of anthracene in the presence of 100 mM TBAX as the supporting electrolyte.[20,47]

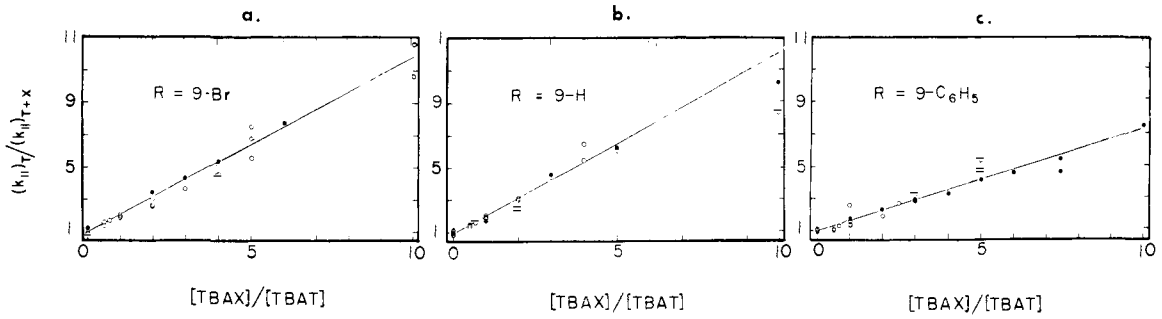

Figure 11. Proof of the "special salt" effect according to eq 11 for (a) 9-bromo-, (b) unsubstituted, and (c) 9-phenylanthracene cations in dichloromethane containing TBAT plus TBAX for X = P (○) and H (●).

rate constant $k_X \gtrsim 1 \times 10^{10}$ M^{-1} s^{-1}. In other words, the rate of ion-pair exchange in eq 10 is also essentially a diffusional process.[48]

The sharp decrease in the rate of the second-order process in the presence of 10 mM TBAP represents an approximately 30-fold retardation relative to that observed in the absence of salt. [For example, with R = H, $k_{III} = 5.8 \times 10^9$ and 1.55×10^{11} M^{-1} s^{-1} with and without TBAP, respectively.] An effect of such a magnitude cannot be accommodated by an ordinary salt effect, especially when a decrease of only 25% is observed with the structurally related salt TBAT at concentrations of 0.1 M (vide supra, Figure 10). The partitioning of A^+ (and T^-) between the active ion pair and the unreactive ion pair as in eq 10 provides a ready mechanism to explain the high sensitivity of the ion-pair decay to the presence of otherwise innocent salts.[25] In solvolysis mechanisms, the enhanced reactivity by innocent salts such as TBAX has been described as the "special salt" effect.

The special salt effect can be quantitatively evaluated by the simultaneous addition of the common ion salt TBAT and the innocent salt TBAX at concentrations sufficient to ensure the complete association of A^+ as ion pairs (vide supra). Under these conditions, the ratio of the first-order rate constants obtained in the presence of TBAT alone (Figure 10) to those obtained in the presence of both TBAT and TBAX (to maintain a constant salt level) is given by eq 11.[50,51] Indeed the plots of this rate-constant

$$\frac{(k_{II})_T}{(k_{II})_{T+X}} = 1 + \frac{k_X[\text{TBAX}]}{k_T[\text{TBAT}]} \qquad (11)$$

ratio against the salt ratio for the three cations in Figure 11 all show intercepts close to unity. The slopes are evaluated as 1.1 for R = H and Br, and ~0.7 for R = C_6H_5 and CH_2=CH. Furthermore, there is no distinction between X = perchlorate and hexafluorophosphate, thus revealing no counterion specificity. The slopes close to unity indicate that $k_T \simeq k_X$, as expected for large ions separated by the long distances appropriate for loose ion pairs. In this context, we note that an association constant of 36×10^3 M^{-1} has been independently measured conductometrically for TBAP in dichloromethane at 20 °C.[52] This value compares with the association constant $K_3 \simeq 30 \times 10^3$ M^{-1} which we have evaluated for $[A^+//T^-]$ in Table X. Effects related to ion pairing at the intimate ion-pair stage may be the cause of small differences in the apparent values of K_3 and k_T/k_X. Curvature of the plots in Figure 11 are observed at higher salt ratios (>10). The deviation from eq 11 could be the result of salt aggregation[53] and/or competition from alternative reactions of A^+ which are allowed by the suppression of the active ion pairs.[54,55]

V. Solvent Effects on Ion-Pair Dynamics. The solvent effects on the ion-pair dynamics are revealed in at least six different ways, as shown by the comparison of benzene, dichloromethane, and acetonitrile representing prototypical apolar, nonpolar, and polar solvents.

In acetonitrile, the second-order rate constants k_{III} (Table VII) for 9-substituted anthracene cations are consistently slower than those measured in dichloromethane (Table IV) by roughly 2 orders of magnitude. Importantly, acetonitrile has a pronounced leveling effect on k_{III}, which are all grouped at about the same value (log $k_{III} \sim 5.1 \pm 0.4$). This limiting value is the same as the second-order rate constant k_{III} for the most persistent cations in dichloromethane, viz., those derived from the meso-substituted derivatives such as 9,10-dimethyl- and 9,10-diphenylanthracene. Taken together, these results indicate that acetonitrile promotes extensive ion-pair dissociation such that reassociation becomes rate-limiting for all A^+. This conclusion is supported by the observation that k_3 mentioned above for the most persistent cations in dichloromethane is singularly unresponsive to either the "common ion" or the "special salt" effect.[56]

The same limiting value of k_{III} is also obtained with arene cations derived from 9-substituted anthracenes in dichloromethane upon the addition of the innocent salts TBAX (compare Tables V and IV). Under these conditions, ion-pair exchange in Scheme III interconverts active ion pairs such as $[A^+//T^-]$ to the inactive ones $[A^+//X^-]$,[46] which is kinetically tantamount to ion-pair dissociation.[48] The chemical consequences of relatively high concentrations of free ions and inactive ion pairs on product formation are presented separately in the Experimental Section.

On the other hand, few free ions exist in the apolar solvent benzene, since even the most persistent arene cations such as those derived from 9,10-dimethyl- and 9,10-diphenylanthracene decay by largely first-order processes and phase III is essentially absent. It is noteworthy that the first-order rate constant k_{II} for the decay of the loose ion pair in benzene is 2 orders of magnitude slower than that observed with more reactive monosubstituted counterparts in dichloromethane, as indicated by a comparison of the results in Tables VIII and III, respectively. This difference is the same as that observed in k_{III} for these two series of arene ions (compare the results in Table IV). Such a dichotomy may arise in disubstituted anthracenes from intrinsically lower reactivities of the ion pairs which experience less of a solvent effect than the "free" ions. Furthermore, the second-order kinetics observed in the special salt effect by TBAP in benzene relates to the formation of inactive ion pairs (see eq 10) in the manner described above for their more reactive counterparts in dichloromethane.

(47) Parker, V. D. *Acc. Chem. Res.* **1984**, *17*, 243 and references therein.
(48) The exchange of counterions in solvent-separated ion pairs might be expected to occur at rates similar to, or somewhat greater than, the rates of encounter of unchanged species owing to the additional quadrupolar interaction in the transition state.[49] The manifestation of second-order kinetics possibly indicates rate-limiting counterion exchange (i.e., $k_T[TBA^+//T^-]$).
(49) Grunwald, E.; Highsmith, S.; T.-P. I., ref 1d, Vol. 2, Chapter 5, pp 447–519.
(50) See Experimental Section for the derivation of eq 11.
(51) Even at molar ratios [TBAT]/[TBAP] as low as 0.01 at [total salt] = 0.1 M, the decay profile is best fitted by a first-order treatment. At lower ratios, the fit to first-order kinetics deteriorates.
(52) Pepper, D. C., private communication cited by J. Smid in ref 45.
(53) Cf.: Goodson, B. E.; Schuster, G. B. *J. Am. Chem. Soc.* **1984**, *106*, 7254.
(54) Such as the reaction of A^+ with NO_2. See: (a) Perrin, C. L. *J. Am. Chem. Soc.* **1977**, *99*, 5516. (b) Eberson, L.; Radner, F. *Acta Chem. Scand., Ser. B* **1980**, *B34*, 739. (c) Schmitt, R. J.; Ross, D. S.; Buttrill, S. E., Jr. *J. Am. Chem. Soc.* **1981**, *103*, 5265.
(55) It is also possible that a small component of the second-order process contributes to the decay profile at the low ratios of [TBAT]/[TBAP].[51]
(56) Thus, under conditions in which the presence (10–20 mM) of either TBAX or TBAP has a profound effect on k_{III} for 9-substituted anthracene cations, the values for k_{III} for the 9,10-disubstituted counterparts are unchanged. (Compare the results in Tables IV, V, and VI).

A consistent pattern of ion-pair behavior thus emerges with the rather subtle variation of the solvent. How the anthracene cation behaves in a given solvent is strongly dependent on its reactivity (as modulated by meso substituents[35,36]). For example, an electron-poor cation such as that derived from 9-nitroanthracene hardly survives the intimate ion-pair stage in acetonitrile, as indicated by $F_{III} \leq 0.2$ in Table VII. On the other hand, an electron-rich cation such as that derived from 9,10-diphenylanthracene is completely dissociated even in the much less polar dichloromethane ($F_{II} = 1.0$ in Table IV). The ion-pairing behavior is a balance between cation reactivity and solvent polarity. Thus, the importance of ion pairing of an electron-poor cation in a polar solvent is more or less equivalent to that of an electron-rich cation in a nonpolar solvent.

VI. Radical-Pair Dynamics. A Comparison. The disappearance of the hydroanthryl intermediate I according to eq 4 represents the dynamics of radical–radical combination. As such, it can be used as a benchmark for the evaluation of the foregoing ion-pair interactions in the absence of charge neutralization.[57] Viewed in this way, the second-order rate constants k_{IV} in Table IX are singularly unaffected by (a) the 9-substituent R or anthracene, (b) the solvent polarity, and (c) the presence of salt.

In order to make a direct comparison between the experimental ion-pair and radical-pair rate constants (i.e., k_{III} and k_{IV} in Table IV and IX, respectively), they must be converted into common units (M^{-1} s^{-1}). Taking the best estimate of the extinction coefficient for the hydroanthryl radical, we evaluate the rate constant k_4 for radical combination (eq 4) to be $\sim 5 \times 10^8$ M^{-1} s^{-1}.[58] This rate constant is about 300 times smaller than that for the related ion combination (eq 3) and 30 times smaller than the rate of diffusional encounter ($k_d \simeq 1.5 \times 10^{10}$ M^{-1} s^{-1})[59] of neutral species.[60] The rate constant k_4 is also smaller than that relevant to the combination of simple organic radicals,[61] which may be attributed to steric interactions at the hindered 9-positions and the lower intrinsic reactivity of the benzylic delocalized radical I. Our attempts to obtain direct measures of k_4 under pseudo-first-order conditions are precluded by the facile thermal reaction of nitrogen dioxide with the anthracenes.[62]

Summary and Conclusions

The charge-transfer excitation of the EDA complex of a series of anthracene donors with tetranitromethane generates the intimate ion pair [A^+,T^-] specifically and directly, which is well-suited for the quantitative study of ion-pair and radical-pair dynamics. Time-resolved spectroscopic studies allow the observation of the ion pairs through three distinct stages, each characterized by its unique decay profile. The kinetic behavior at each stage identifies (a) the intimate ion pair (rapid first-order decay, $k_1 \sim 10^9$ s^{-1}), (b) the "loose" or solvent-separated ion pair (slower first-order decay, $k_2 \sim 10^7$ s^{-1}), and (c) the "free" ions (second-order decay, $k_3 = 10^{11}$ M^{-1} s^{-1}), as originally formulated for solvolysis mechanisms. The formation of loose ion pairs as described by Winstein and co-workers is substantiated by the quantitative treatment of the "special salt" effect induced by innocent salts such as TBAP and TBAH. Similarly, the interception of ion pairs by TBAT provides a quantitative basis of the "common ion" effect. This extreme sensitivity of ion-pair reactivity to salts as well as to solvent polarity and charge delocalization stands in strong contrast to the corresponding radical-pair reactivity of the neutral hydroanthryl intermediate I, which is singularly unaffected by all these influences. Furthermore, the ion-pairing behavior of the ions A^+ and T^- is remarkably similar to that observed with the ions derived from solvolysis.[64]

The generality of the ion-pairing phenomenon derives from the dominance of the inherent Coulombic interaction. However, specific dynamics will depend on the nature of the ions involved, especially at the intimate ion-pair stage.[65] Similarly S_N1 reactivity in solvolysis is dependent on charge stabilization and solvent polarity. Such a parallel suggests that loose ion pairs may generally be the preferred species in solution under ion-pairing conditions for solvolysis. Analogous processes undoubtedly pertain to electron-transfer quenching of photoexcited states, in which salt effects have also been observed.[66,67] Charge-transfer excitations of EDA complexes enjoy the advantage over quenching techniques in producing geminate ion pairs directly and specifically without diffusional ambiguities. Thus, ions derived by quenching may be produced at the loose ion pair stage[66] or even at larger separations by exergonic electron transfer over long distances.[68] The greater probability of escape from loose ion pairs may in part explain the generally higher quantum yields for ionic reactions derived by sensitization in comparison to those obtained by excitation of the EDA complex.

Experimental Section

Materials. 9,10-Dichloroanthracene (Aldrich) was recrystallized from alcohol. 10-Methyl-9-anthraldehyde and 9-vinylanthracene (Aldrich) were used as received. Procurement and purification of the other anthracene derivatives has been described previously.[18,20] Tetranitromethane[69] and nitroform[70] were prepared by literature methods. Dichloromethane (Aldrich, Gold Label), acetonitrile (Fisher), methanol (Mallinckrodt), benzene (Mallinckrodt), and cyclohexane (Matheson) were used as received.

Tetra-*n*-butylammonium perchlorate (G. F. Smith Co.) and tetra-*n*-butylammonium hexafluorophosphate (Ozark Mahoning) were recrystallized from a mixture of isooctane and ethyl acetate and from absolute ethanol, respectively. They were further dried under vacuo. Tetranitromethide salts were prepared from nitroform[70] in the following manner.

Benzyltrimethylammonium Trinitromethide. Nitroform (3.3 g) was dissolved in 50 mL of ethanol and the solution cooled in an ice bath. A 40% solution (Marschall Chemical) of benzyltrimethylammonium hydroxide in methanol (9.8 mL) as added dropwise with swirling. Approximately 15 min after the addition was complete, a yellow precipitate formed. This precipitate was collected by vacuum filtration, washed with ether, and dried in air: yield 2.1 g (32%); ^1H NMR (in $CDCl_3$) (TMS) δ 7.50 (s, 5 H), 4.54 (s, 2 H), 3.17 (s, 9 H); UV (CH_2Cl_2) λ_{max} 351 nm (ϵ_{max} 13 760); IR (KBr) 3049, 3008, 2967, 2361, 2338, 1500, 1384, 785, 730 cm^{-1}. The pure compound was unstable in the solid even at −15 °C and underwent decomposition with the explosive release of gases when stored in the dark at room temperature. Caution should be exercised when working with any trinitromethide salt.

Tetrabutylammonium Trinitromethide. A measured amount (7.25 g) of a 55% solution of tetrabutylammonium hydroxide (Chemical Dynam-

(57) Based only on a consideration of the roughly equal sizes of the reacting ions and radicals.

(58) We take an average of $\epsilon_{rad} \simeq 2000$ M^{-1} cm^{-1} for the hydroanthryl radical[17] and k_{IV} $\epsilon_{rad}l$.

(59) See: (a) ref 37 and: (b) Masnovi, J. M.; Korp, J. D.; Kochi, J. K.; Hilinski, E. F.; Rentzepis, P. M. *J. Phys. Chem.* in press.

(60) A statistical production of triplet and reactive single radical ion pairs in the ratio of three to one would result in k_4 to be less than k_d. CIDNP was not observed during these reactions (Closs, G. L., private communication).

(61) (a) The second-order rate constants for the combination of pentyl and benzyl radicals are 1.0×10^9 and 4.1×10^9 M^{-1} s^{-1}. Burkhart, R. D. *J. Am. Chem. Soc.* **1968**, *90*, 273. (b) Diarylcarbenes dimerize in benzene with second-order rate constants of $1.1–5.4 \times 10^9$ M^{-1} s^{-1}. Closs, G. L.; Robinow, B. E. *J. Am. Chem. Soc.* **1976**, *98*, 8190.

(62) (a) Cf.: Pryor, W. A.; Gleicher, G. J.; Cosgrove, J. P.; Church, D. F. *J. Org. Chem.* **1984**, *49*, 5189. (b) Thus, at this juncture, we are unable to state with certainty whether k_{IV} measures the reaction of I with only NO_2 as in eq 4 but also with the dimeric N_2O_4. [The rate of dimerization of NO_2 is thought to exceed 10^6 M^{-1} s^{-1}.][63] However, at the concentrations ($\sim 10^{-5}$ M) of NO_2 produced in our experiments, the equilibrium fraction existing as N_2O_4 is ~20%, and the correction for the dimerization should not greatly affect the value of k_{IV}.

(63) (a) Pryor, W. A.; Castle, L.; Church, D. F. *J. Am. Chem. Soc.* **1985**, *107*, 211. (b) See Redmond, T. F.; Wayland, B. B. *J. Phys. Chem.* **1968**, *72*, 1626. And see ref 62 for the dissociation constant of N_2O_4 which leads to the dissociation rate as $>2 \times 10^2$ s^{-1}.

(64) In this respect, the "radical" character of the anthracene cation radical is not influential.

(65) For the structural considerations inherent in tight or inner-sphere ion pairs. See: Fukuzumi, S.; Kochi, J. K. *J. Phys. Chem.* **1980**, *84*, 609. And compare with outer-sphere ion pairs (Fukuzumi, S.; Wong, C. L.; Kochi, J. K. *J. Am. Chem. Soc.* **1980**, *102*, 2928).

(66) Weller, A. *Pure Appl. Chem.* **1982**, *54*, 1885.

(67) (a) Mataga, N. *Pure Appl. Chem.* **1984**, *56*, 1255. (b) McCullough, J. J.; Veroushalmi, S. *J. Chem. Soc., Chem. Commun.* **1983**, 254. And see ref 53.

(68) Calcaterra, L. T.; Closs, G. L.; Miller, J. R. *J. Am. Chem. Soc.* **1983**, *105*, 670.

(69) Liang, P. "Organic Synthesis"; Wiley: New York, 1955; Collect. Vol. 3, p 803.

(70) Homer, J.; Huck, P. J. *J. Chem. Soc. A* **1968**, 277.

ics) in water was added dropwise to an alcoholic solution of 7.7 g of nitroform as described above. The precipitate was collected, washed with ether, and recrystallized from a mixture of methanol and water. It was dried over anhydrous calcium sulfate and potassium hydroxide pellets: yield 5.5 g (28%); ^{1}H NMR (in $CDCl_3$) (TMS) δ 3.13 (t, 2 H), 1.47 (m, 4 H), 0.99 (t, 3 H); UV (CH_2Cl_2) λ_{max} 352 nm (ϵ_{max} 12 700); IR (KBr) 2967, 2877, 1535, 1488, 1384, 1266, 1156, 785, 733 cm^{-1}. Anal. Calcd for $C_{17}H_{36}N_4O_6$: C, 52.03; H, 9.25; N, 14.28. Found: C, 52.00; H, 9.28; N, 14.25.

Instrumentation. Electronic spectra were obtained on a Hewlett-Packard 8450 A diode array spectrophotometer. Infrared spectra were taken on a Nicolet 10DX FTIR spectrometer. NMR spectra were recorded with the aid of a JEOL FX 90Q 90-MHz spectrometer.

Time-resolved differential absorption spectra on the nanosecond time scale were obtained with the 532-nm second harmonic, 200-ns pulse from a Quantel Nd:YAG laser excitation source. A pulsed xenon flashlamp mounted perpendicular to the excitation beam was used in conjunction with a Spex Minimate monochromator, Hanamatsu R928 NM tube, and Tektronix R7912 digitizer for the probe assembly.[71] Time-resolved spectra on the microsecond time scale were obtained on a system utilizing the 532-nm second harmonic, 10-ns pulses from a Quantel YG481 Nd:YAG laser which was monitored with a conventional xenon lamp, monochromator, and photomultiplier arrangement. Digitized signals were interfaced with a Digital Equipment PDP 11/70 computer for analysis.[72]

Ion Pair Kinetics. The reaction order of the kinetics was established by linear least-squares computer fit of the observed decrease of the absorbance (A) with time as a function of either ln A or A^{-1} for first or second order, respectively. The random distribution of the residuals over 4–5 half-lives (when possible) was used for the assignment of the kinetics order, and it allowed a ready discrimination between simple first- and second-order decays upon comparison of several runs at different concentrations, light intensities, and slit widths. More complicated decays (e.g., see Figure 2) could be deconvoluted by sequential analysis by determining the rate of the slower component initially. In this way, the third decay was found to follow entirely (>95%) second-order kinetics.

These experimental decays are related to the microscopic rate constants in the following way:

Phase I. On the picosecond time scale, the kinetics scheme is

$$\mathbf{I} \xleftarrow{k_1} [A^+,T^-] \xrightarrow{k_{-2}} [A^+//T^-] \tag{12}$$

and slower processes can be neglected. The total absorbance A_λ measured at a wavelength (690 nm < λ < 730 nm) where **I** does not absorb is

$$A_\lambda = A_i + A_s$$

where the subscripts i and s hereafter refer to the intimate ion pair $[A^+,T^-]$ and the solvent-separated ion pair $[A^+//T^-]$, respectively. The observed change in absorbance is

$$\frac{dA_\lambda}{dt} = \frac{dA_i}{dt} + \frac{dA_s}{dt} \tag{13}$$

If the extinction coefficient for both ion pairs is the same as that of the free ion[21] (f), i.e.,

$$\epsilon_i = \epsilon_s = \epsilon_f = \epsilon \tag{14}$$

(note the similarity of the absorption spectra in ref 14 and 15 measured after 25 ps, with those in Figure 1), then

$$\frac{1}{\epsilon l}\frac{dA_\lambda}{dt} = \frac{d[A^+,T^-]}{dt} + \frac{d[A^+//T^-]}{dt}$$

From eq 12,

$$\frac{d[A^+,T^-]}{dt} = -(k_1 + k_{-2})[A^+,T^-]$$

$$\frac{d[A^+//T^-]}{dt} = k_{-2}[A^+,T^-]$$

so that

$$\frac{1}{\epsilon l}\frac{dA_\lambda}{dt} = -k_1[A^+,T^-] \tag{15}$$

Thus, the absorbance change should show a first-order dependence on $[A^+,T^-]$. A plot of the absorbance changes in the picosecond data in ref 15 and 17 appeared linear with a slope of 1.3×10^9 s^{-1} for the anthracene cation radical.[73] However, since it was not apparent that the integrated form of eq 15 would afford a single exponential dependence of A with time (owing to the nonlinear differential eq 13), we also extracted the rate constants by an alternative procedure. For a given decay curve, the value of $F_{II} = F_2 = k_{-2}/(k_1 + k_{-2})$ should be invariant with time (since solvent and vibrational relaxation processes have shorter correlation times).[14] The absorbance due to $[A^+,T^-]$ was then obtained by multiplying the overall decay by $(1 - F_2)^{-1}$, i.e.,

$$\frac{d[A^+,T^-]}{dt} = \frac{1}{\epsilon l}\frac{d(1 - F_2)^{-1}A_\lambda}{dt} = -(1 - F_2)^{-1}k_1[A^+,T^-] = -(k_1 + k_{-2})[A^+,T^-] \tag{16}$$

Integration of eq 16 leads to $(k_1 + k_{-2})$ by routine first-order analysis. The value of $k_1 = 1.5 \times 10^9$ s^{-1} obtained by this procedure (Table V) is easily within experimental error of that obtained in the manner described above. The kinetics analysis for the other derivatives reported in Table II was straightforward since $k_1 \gg k_{-2}$.

Phase II. On the nanosecond time scale, the equilibration between $[A^+,T^-]$ and $[A^+//T^-]$ is established, and $[A^+,T^-]$ was assumed to be in a steady-state condition for the kinetics scheme

$$\mathbf{I} \xleftarrow{k_1} [A^+,T^-] \underset{k_2}{\overset{k_{-2}}{\rightleftharpoons}} [A^+//T^-] \xrightarrow{k_{-3}} A^+ + T^- \tag{17}$$

External return (k_3) was neglected owing to the low concentration of free ions under these conditions. Then

$$A_\lambda = A_i + A_s + A_f$$

and

$$\frac{1}{\epsilon l}\frac{dA_\lambda}{dt} = \frac{d[A^+,T^-]}{dt} + \frac{d[A^+//T^-]}{dt} + \frac{d[A^+]}{dt} \tag{18}$$

with

$$\frac{d[A^+,T^-]}{dt} = -(k_1 + k_{-2})[A^+,T^-] + k_2[A^+//T^-] = 0 \tag{19}$$

$$\frac{d[A^+//T^-]}{dt} = -(k_2 + k_{-3})[A^+//T^-] + k_{-2}[A^+,T^-]$$

$$\frac{d[A^+]}{dt} = k_{-3}[A^+//T^-]$$

and eq 15 is valid. From eq 15 and 19,[34b]

$$\frac{1}{\epsilon l}\frac{dA_\lambda}{dt} = -\frac{k_1k_2}{k_1 + k_{-2}}[A^+//T^-] \tag{20}$$

The rate constant $k_{II} = k_1k_2(k_1 + k_{-2}) = k_2(1 - F_{II})$ can then be derived as described for phase I. For anthracene and 9-bromoanthracene, the absorptions due to both $[A^+,T^-]$ and $[A^+]$ are small compared to those of $[A^+//T^-]$, and the same result is obtained from either method. For the 9-phenyl and 9-vinyl analogues, $[A^+]$ is substantial. Nonetheless, the values of k_{II} differed only by about 20%. [The higher values resulted from the approximation using the subtraction procedure typically illustrated in Figure 2, which overestimates the absorption of $[A^+]$ at early times but is compensated for by the neglect of k_{-3}.] The standard deviation in the fits of k_{II} to the observed decays and in F_{II} were 10–20%. Thus, the simpler spectral subtraction procedure was adequate (within the experimental uncertainty) to demonstrate the general circumstances and effects of association into loose ion pairs. The values reported in Table III were obtained by this approximate method.

Phase III. On the microsecond time scale, the equilibrium among $[A^+,T^-]$, $[A^+//T^-]$, and $[A^+]$ is established, and both ion pairs can be treated as though they were in steady state. From eq 15 and 19–21,

$$\frac{d[A^+//T^-]}{dt} = -(k_2 + k_{-3})[A^+//T^-] + k_{-2}[A^+,T^-] + k_3[A^+][T^-] = 0 \tag{21}$$

and

$$\frac{d[A^+]}{dt} = -k_3[A^+][T^-] + k_{-3}[A^+//T^-] \tag{22}$$

(71) See: Atherton, S. J. *J. Phys. Chem.* **1984**, *88*, 2840.
(72) Foyt, D. C. *J. Comput. Chem.* **1981**, *5*, 49.

(73) Similarly, the value of k_1 was apparently obtained in ref 10b from the first-order analysis of ln A vs. time for the decay of an intimate ion pair by competition between reverse electron transfer and relaxation to a loose ion pair.

we derive

$$\frac{1}{\epsilon l}\frac{dA}{dt}\lambda = \frac{k_1k_2k_3}{k_{-3}(k_1 + k_{-2}) + k_1k_2}[A^+][T^-] = k_{III}[A^+]^2 \quad (23)$$

since $[A^+] = [T^-]$. Algebraic rearranging and substituting F_2 and $F_3 = k_{-3}/(k_2 + k_{-3})$ affords eq 7.

Spectral Measurements. Solutions of 0.05 M anthracene and 0.1 M tetranitromethane were placed in a 1.0 × 0.5 cm stoppered cuvette and deaerated with a slow stream of nitrogen. Intensity calibrations used hematoporphyrin IX (ϵ_{440} = 14 000 M^{-1} cm^{-1}, ϕ_{isc} = 0.83 in 90% aqueous methanol),[74] the concentration of which was adjusted to give the same absorbance at 532 nm as the EDA complexes. Values obtained for the rate constants and intensities represent averages of between 5 and 16 experiments on independent samples. In each experiment, between 6 and 15 shots were averaged to obtain a single trace. The solutions were frequently replenished to minimize degradation. The kinetics were independent of the concentrations of the anthracene and TNM between 0.02 and 0.2 M. At relatively high concentrations of anthracene (>0.03 M), the kinetics were somewhat complicated by the formation of π-dimer cation radicals.[59b] The decays were also unaffected by either an increase or decrease of the intensity of the incident light by a factor of ~4. The presence of air did not noticeably affect the decays of either the anthracene cations or the hydroanthryl radicals **I**.

The anthracene cations were found to be relatively inert toward weak nucleophiles. Indeed the decays of A^+ were in fact greatly decreased when the dichloromethane solvent was diluted with methanol owing to an increase in solvent polarity. The decays in neat methanol were comparable to those in acetonitrile. Addition of nonpolar solvents such as benzene or cyclohexane greatly reduced the amount of free ions undergoing cage escape. In neat benzene or cyclohexane, $F_{II} \simeq 0$ for the monosubstituted anthracenes. Radical cations of 9,10-diphenylanthracene and 9,10-dimethylanthracene could be readily detected in these solvents, however. The value for the first-order rate constant k_I for the 9-cyanoanthracene cation in Table II is approximate since it is based on a two-point determination. [We thank P. M. Rentzepis and E. F. Hilinski for these picosecond spectra.]

Extinction coefficients of the anthracene cations are required to convert second-order decays measured in absorption units (A^{-1} s^{-1}) into concentration units (M^{-1} s^{-1}), using Beer's law (l = 0.5 cm). The extinction coefficient of the unsubstituted anthracene cation has been determined by pulse radiolysis.[22] We have taken the same extinction coefficient to apply under our conditions. The values of ϵ_{max} have not been reported for the other anthracene derivatives. Since the absorption spectra of the meso-monosubstituted anthracene cations (R = Br, C_6H_5, CH_2=CH, CN, and NO_2) resemble that of the anthracene cation, we have assumed the same value of ϵ_{max} for these species. On the other hand, the absorption spectra of the cations of 9-methoxyanthracene and the meso-disubstituted anthracenes appear quite different from that of anthracene cation (cf. Figure 1). It is also likely that the ϵ_{max} differ. The low rate observed for the decay of these species, coupled with the large values of F_{III} (~1.0), and the lack of a dependence of the rates and absorptions on solvent or added salts (Tables VII and VIII) imply high values of F_{II} for these species. Accordingly, we have calculated ϵ_{max} from the calibration data of these compounds assuming a uniform value for F_{II} of unity (Table I). Second-order decays in concentration units were obtained from the observed decays by using these values of the extinction coefficients.

For the determination of F_{II}, the intensity of the incident light was determined by using hematoporphyrin IX (vide supra), the concentration of which was adjusted to give the same absorbance at the wavelength of excitation (532 nm) as the EDA complex. The concentration of anthracene cations present after ~10 ns was determined as $[A^+] = A_{10ns}/(\epsilon_{max}l)$ from the nanosecond decay profiles at λ_{max}. The ratio of cations remaining after 4 ns to that produced by 532-nm excitation (F_{II}) was calculated from the ratio of the concentrations of A^+ relative to that of hematoporphyrins triplet $[HP]_t$, i.e.

$$[A^+]_{10ns}/[A,TNM]_{excited} = [A^+]_{10ns}\phi_{ions}^{-1}([HP]_t\phi_{isc}^{-1})^{-1}$$

where the quantum yield of formation of intimate ion pairs ϕ_{ions} was assumed to be unity. [Values of $\phi_{-A} \simeq 0.8$ have been measured.[15,17]]

In Figures 4a and 8a, the decays ascribed to **I** and A^+ appear to be similar, as indicated by the values of k_{II} (Tables IV and VII) and k_{IV} (Table IX). However, note the difference in the extinction coefficients of **I** and A^+ upon which the microscopic rate constants are dependent in second-order reactions. Furthermore, the rates of decay of **I** and A^+ in Figure 4b and 8b are clearly different. The overlapping absorptions complicate the kinetics analysis. In the case of electron-rich cations in polar solvents, we cannot exclude the possibility of reversible formation of **I** (i.e., $k_{-1} \neq 0$). For an alternative explanation, see the product studies in the next section.

(74) Reddi, E.; Jori, G.; Rodgers, M. A. J.; Spikes, J. D. *Photochem. Photobiol.* **1983**, *38*, 639.

Table XI. Solvent and Salt Effects on the Product Yields of Photoadducts **II**[a]

9-R-,10-R-anthracene	dichloromethane			acetonitrile	hydrocarbon
	no salt	TBAP[b]	TBAT[b]		
Br, H	80	76	87	65	86[c]
C_6H_5, H	64		75	21	85[d]
H, H	15	5	26	5	37[e]
CH_2=CH, H[f]	60		62	55	58[d]
CH_3, CH_3	15	12	8		43[g]

[a] As % yield (±10%) based on A. Determined by ^1H NMR analysis at either 90 or 360 MHz.[18] [b] 0.1 M. [c] Cyclohexane. [d] Cumene. [e] Methylcyclohexane. [f] Adduct may be an isomer of **II** in which NO_2 is attached to the vinylic terminus. [g] Pentane.

Product Studies. In order to augment the kinetics study of ion-pair decay with the attendant chemistry, we examined the yields of the photoadducts **II** under relevant conditions of the solvent changes and the salt additions summarized in Table XI. The 9-substituted anthracenes with electron-withdrawing substituents (e.g., R = NO_2 and Br) typically afford adducts **II** in high yields irrespective of the solvent polarity or the presence of salt. On the other hand, the 9-substituted anthracenes with electron-releasing substituents (e.g., R = H and Ph) afford mixtures of products, the compositions of which are more dependent on the solvent, salt, and temperature. Part of the problem in the latter case lies with the difficulty in the isolation of the photoadducts **II** as a result of their enhanced thermal lability.[18] Furthermore, the hydroanthryl adduct **I** derived from electron-rich anthracenes is also subject to further oxidation, the resulting products of which we have reported separately.[18] The results in Table XI suggest that the yields of photoadducts **II** from electron-rich anthracenes are most adversely affected by the polar solvent acetonitrile and the innocent salt TBAP. These are also conditions which we find to lead to either extensive ion-pair dissociation or counterion exchange to inactive ion pairs. (See the Discussion section for solvent and special salt effects, respectively.) Under these conditions, the reaction of the arene cation with T^- is slow, and the reaction of the longer-lived species with NO_2 may become competitive. [Note that the decay of A^+ in acetonitrile or in dichloromethane with TBAT levels off at about the same rate (~10^9 M^{-1} s^{-1}) which is similar to that observed for the combination of the hydroanthryl intermediate **I** with NO_2]. Anthracene reacts with NO_2 with a second-order rate constant 2.2 × 10^3 M^{-1} s^{-1} at 25 °C in dichloromethane to afford 9-nitroanthracene and anthraquinone.[62] The anthracene cation as an open-shell species is expected to be even more reactive with NO_2.[54] Thus, the arene cation, either as A^+ or $[A^+//X^-]$, can react with NO_2 under conditions in which the reaction with T^- is sufficiently suppressed. Such a competition is most likely to arise with the electron-rich meso-disubstituted anthracenes such as the 9,10-dimethyl and 9,10-diphenyl derivatives. In these cases, ion-pair escape for the solvent cage appears to be complete ($F_{II} \simeq 1.0$ in Table IV). The decay profile of these persistent cations is the same in acetonitrile as it is in dichloromethane, and added TBAP and TBAT have no effect. [9,10-Dimethylanthracene cation persists for >1 s when it is generated electrochemically in dichloromethane containing 0.1 M TBAP.[59b]] The formation of the side-chain substitution product in eq 12 may arise from such an interaction, i.e.

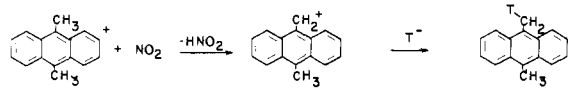

(24)

Such reactions of NO_2 might generally become competitive whenever the rate of ion-pair collapse of $[A^+//T^-]$ diminishes owing to the reduced impetus for charge annihilation in stabilized arene cations.

Derivation of Equation 6. The loose ion pair dissociates (fraction F_{III}) to form free ions, and it re-forms the tight ion pair (fraction $1 - F_{III}$). That part re-forming the tight ion pair relaxes (fraction F_{II}, total $[1 - F_{III}]F_{II}$) again to the loose ion pair, and this cycle continues. The total amount of solvent-separated ions which ultimately becomes "free" to decay with second-order kinetics (F_{III}) can be expressed as

$$F_{III} = F_3 + (1 - F_3)F_2F_3 + (1 - F_3)F_2(1 - F_3)F_2F_3 + \ldots \quad (25)$$

$$F_{III} = F_3\{1 + (1 - F_3)F_2 + [(1 - F_3)F_2]^2 + \ldots\} \quad (26)$$

$$F_{III} = F_3\sum_{n=0}^{\infty}[F_2(1 - F_3)]^n \quad (27)$$

Since this is a power series, the total is given by

$$F_{III} = F_3[1 - F_2(1 - F_3)]^{-1} \quad (6)$$

We find for R = H, $F_3 = 0.13$ and $F_{III} = 0.20$, R = Br, $F_3 = 0.13$ and $F_{III} = 0.20$, R = C_6H_5, $F_3 = 0.13$ and $F_{III} = 0.32$, and R = C_2H_3, $F_3 = 0.21$ and $F_{III} = 0.41$.

Derivation of Equation 11. Note from Scheme II that

$$K_3 = k_3/k_{-3} = [A^+//T^-]/[A^+][T^-] \simeq 2 \times 10^4\ M^{-1} \quad (28)$$

$$K_3' = k_3'/k_{-3}' = [A^+//X^-]/[A^+][X^-] \quad (29)$$

$$K_a = k_a/k_{-a} = [TBA^+//T^-]/[TBA^+][T^-] \quad (30)$$

$$K_a' = k_a'/k_{-a}' = [TBA^+//X^-]/[TBA^+][X^-] \simeq 3.6 \times 10^4\ M^{-1} \quad (31)$$

$$k_X/k_T = [A^+//X^-][TBA^+//T^-]/[A^+//T^-][TBA^+//X^-] = \frac{K_3'}{K_3}\Big/\frac{K_a'}{K_a} \quad (32)$$

The rate of reaction from the loose ion pair $[A^+//T^-]$ (steady-state assumption for the intimate ion pair with $k_0 = k_1k_2[k_1 + k_{-2}]^{-1}$) is

$$-\frac{d[A^+]}{dt} = k_0[A^+//T^-] = k_0\frac{[A^+//T^-]}{[A^+]_0}[A^+]_0 \quad (33)$$

where $[A^+]_0 = [A^+//T^-] + [A^+//X^-] + [A^+]$ is the total concentration of A^+ present. If only $[A^+//T^-]$ is reactive,

$$k_{II} = k_0\frac{[A^+//T^-]}{[A^+]_0} \quad (34)$$

At sufficient concentrations of added salt to ensure complete ion pairing of A^+ (i.e., $[A^+] \simeq 0$), then $[A^+]_0 = [A^+//T^-]$ when TBAT alone is added, and $[A^+] = [A^+//T^-] + [A^+//X^-]$ when both TBAT and TBAX are added together. Hence,

$$\frac{(k_{II})_T}{(k_{II})_{T+X}} = \frac{k_0}{k_0\dfrac{[A^+//T^-]}{[A^+//T^-] + [A^+//X^-]}} = 1 + \frac{[A^+//X^-]}{[A^+//T^-]} \quad (35)$$

For $[TBA^+] \gg [A^+]$, $[TBA^+//T^-] \simeq$ [TBAT] added and $[TBA^+//X^-] \simeq$ [TBAX] added. Substituting eq 32 into eq 35 yields

$$\frac{(k_{II})_T}{(k_{II})_{T+X}} = 1 + \frac{k_X}{k_T}\frac{[TBAX]}{[TBAT]} \quad (11)$$

Acknowledgment. We thank S. J. Atherton and M. A. J. Rodgers of the Center for Fast Kinetics Research (under support from NIH Grant RR00886 and the University of Texas, Austin) for invaluable help and discussion, A. Levine for technical assistance, and the National Science Foundation and the Robert A. Welch Foundation for financial assistance.

Tailored Excitation for Fourier Transform Ion Cyclotron Resonance Mass Spectrometry

Alan G. Marshall,*[†,‡,⊥] Tao-Chin Lin Wang,[†] and Tom L. Ricca[⊥]

Contribution from the Department of Chemistry, Department of Biochemistry, and Chemical Instrument Center, The Ohio State University, Columbus, Ohio 43210. *Received June 3, 1985*

Abstract: All present FT/ICR instruments operate with single-pulse or frequency-sweep radio frequency excitation waveforms, which produce excitation power with non-uniform amplitude and limited mass selectivity. This paper introduces a general "tailored" excitation time-domain waveform obtained by inverse Fourier transformation of the desired excitation spectrum. The new method includes all other excitation waveforms as subsets and may be operated in direct or heterodyne mode. Major applications include the following: flatter excitation power over the detected mass range, excitation power with one or more windows for suppression of large peaks or for more selective ion ejection for MS/MS, and multiple-ion monitoring with simultaneous detection of any number of selected mass-to-charge ratios. Theoretical and experimental examples of all three types of excitation are given. The method is readily adapted to existing instruments with minor hardware and software modifications.

Since its introduction in 1974,[1,2] Fourier transform ion cyclotron resonance mass spectrometry has advanced to become an extraordinarily versatile mass spectrometric technique whose advantages have recently been reviewed.[3,4] Briefly, its most important features are the following: simultaneous detection of the entire mass spectrum at once (typically in ca. 0.1 s); potentially ultrahigh mass resolution (e.g., 1000000:1 at mass-to-charge ratio, m/z 200); and an upper mass limit that has yet to be reached. Although major progress has been made in improving FT/ICR *detection* (e.g., reducing base pressure to about 10^{-10} torr, extending the bandwidth of the detection circuit, shielding of the transmitter and detector leads, differentially-pumped dual-cell,[5] etc.), there have been no fundamental advances in FT/ICR *excitation* since 1974.

Ideal FT/ICR excitation power spectra (i.e., excitation magnitude as a function of frequency) are shown in Figure 1. For ordinary detection, one might choose perfectly flat excitation power (Figure 1, top trace), in order to excite ions of various m/z values to a common orbital radius,[6] to yield a mass spectrum in which the intensities (areas) of the various peaks accurately reflect the relative numbers of ions at those m/z values.[7] The excitation spectrum shown in the middle trace of Figure 1 consists of flat power over a specified mass range, with a zero-power window of specifiable width. Windowed excitation is useful for suppressing (by failing to excite) a large peak whose presence could make detection of small peaks difficult. Windowed excitation may also be used to eject ions of all but one m/z value; ions at that m/z

[†] Department of Chemistry.
[‡] Department of Biochemistry.
[⊥] Chemical Instrument Center.

(1) Comisarow, M. B.; Marshall, A. G. *Chem. Phys. Lett.* **1974**, *25*, 282–283.
(2) Comisarow, M. B.; Marshall, A. G. *Chem. Phys. Lett.* **1974**, *26*, 489–490.
(3) Marshall, A. G. *Acc. Chem. Res.* **1985**, *18*, 316–322.
(4) Wanczek, K. P. *Int. J. Mass Spectrom. Ion Proc.* **1984**, *60*, 11–60. Gross, M. L.; Rempel, D. L. *Science* **1984**, *226*, 261–268.
(5) Ghaderi, S.; Littlejohn, D. P. 1985 33rd American Society for Mass Spectrometry Annual Conference, San Diego, CA, May, 1985, Paper No. ROC12.
(6) Comisarow, M. B. *J. Chem. Phys.* **1978**, *69*, 4097; see also ref 12.
(7) Comisarow, M. B. *J. Chem. Phys.* **1978**, *69*, 4097–4104.

0002-7863/85/1507-7893$01.50/0